ORIGIN OF COLORATION IN BEETLE SCALES: AN OPTICAL AND STRUCTURAL INVESTIGATION

by

Ramneet Kaur Nagi

A thesis submitted to the faculty of
The University of Utah
in partial fulfillment of the requirements for the degree of

Master of Science

in

Physics

Department of Physics and Astronomy

The University of Utah

December 2014

The University of Utah Graduate School

STATEMENT OF THESIS APPROVAL

The thesis of **Ramneet Kaur Nagi**

has been approved by the following supervisory committee members:

Shanti Deemyad, Chair	8/12/2014 Date Approved
Michael H. Bartl, Co-chair	8/12/2014 Date Approved
Mikhail E. Raikh, Member	8/12/2014 Date Approved

and by **Carleton DeTar**, Chair of the Department of **Physics and Astronomy** and by David B. Kieda, Dean of The Graduate School.

ABSTRACT

In this thesis the origin of angle-independent yellowish-green coloration of the exoskeleton of a beetle was studied. The beetle chosen was a weevil with the Latin name *Eupholus chevrolati*. The origin of this weevil's coloration was investigated by optical and structural characterization techniques, including optical microscopy, scanning electron microscopy imaging and focused ion beam milling, combined with three-dimensional modeling and photonic band structure calculations. Furthermore, using color theory the pixel-like coloring of the weevil's exoskeleton was investigated and an interesting additive color mixing scheme was discovered.

For optical studies, a microreflectance microscopy/spectroscopy set-up was optimized. This set-up allowed not only for imaging of individual colored exoskeleton domains with sizes ~2-10 μm, but also for obtaining reflection spectra of these micrometer-sized domains. Spectra were analyzed in terms of reflection intensity and wavelength position and shape of the reflection features. To find the origin of these colored exoskeleton spots, a combination of focused ion beam milling and scanning electron microscopy imaging was employed. A three-dimensional photonic crystal in the form of a face-centered cubic lattice of ABC-stacked air cylinders in a biopolymeric cuticle matrix was discovered. Our photonic band structure calculations revealed the existence of different sets of stop-gaps for the lattice constant of 360, 380 and 400 nm in the main lattice directions, Γ-L, Γ-X, Γ-U, Γ-W and Γ-K.

In addition, scanning electron microscopy images were compared to the specific directional-cuts through the constructed face-centered cubic lattice-based model and the optical micrographs of individual domains to determine the photonic structure corresponding to the different lattice directions. The three-dimensional model revealed stop-gaps in the Γ-L, Γ-W and Γ-K directions.

Finally, the coloration of the weevil as perceived by an unaided human eye was represented (mathematically) on the *xy*-chromaticity diagram, based on *XYZ* color space developed by CIE (Commission Internationale de l'Eclairage), using the micro-reflectance spectroscopy measurements. The results confirmed the additive mixing of various colors produced by differently oriented photonic crystal domains present in the weevil's exoskeleton scales, as a reason for the angle-independent dull yellowish-green coloration of the weevil *E. chevrolati.*

To my advisor, Dr. Michael H. Bartl, and my parents

CONTENTS

LIST OF FIGURES

ACKNOWLEDGEMENTS

I express my eternal gratitude and heartfelt thanks to my advisor, Dr. Michael H. Bartl, for his constant guidance, unconditional support and patience throughout that made my stint a great learning experience. Dr. Bartl espouses high standards of research and I am very grateful for his scientific advice and insightful discussions and suggestions and the wonderful opportunity he gave me to contribute to this interesting and exciting project. I have greatly benefitted by his intelligence and vast knowledge. I truly appreciate having him as my advisor.

I extend my sincere gratitude to the members of my supervisory committee, Prof. Mikhail E. Raikh and Dr. Shanti Deemyad. I am thankful to Prof. Raikh for providing me with the significant theoretical knowledge through his extremely organized and scholarly lectures that I could apply in my research work. I am very thankful for and appreciative of the continued support, guidance and helpful career direction provided by Dr. Deemyad.

I acknowledge the significant contributions of Dr. Randy Polson in carrying out the focused-ion beam milling experiments on the beetle scales and Ms. Danielle Montanari for her band structure calculations and crystal lattice modeling.

I am thankful for the helpful suggestions and feedback I received from all the members of the Bartl Group, *The Bartl Buddies* (as we call it!). A special thanks to Dr. Aditi Risbud for her guidance and words of encouragement.

Lastly, I would like to thank my family for their endless love, care and constant support.

CHAPTER 1

INTRODUCTION

1.1 Photonic Crystals: Properties and Applications

Researchers have been inspired and determined to explore and solve the mystery behind the brilliant displays of color and chromatic effects found in the animal and plant kingdom.[1, 2] Though many of the observed colors are due to the pigmentation, several insects, birds and marine animals have evolved to produce specific types of *structures* in their exoskeleton, feathers and bodies for the purpose of coloration.[3-9] These *structural colors* are produced by diffraction, specular reflection, and interference of light rather than absorption and diffuse reflection.[8, 10-12] The key to structural colors is a periodic arrangement of dielectric compounds with a periodicity on the order of the wavelength of visible light.[7] Depending upon the periodicity, or lattice parameters, of the structure, certain wavelengths are classically forbidden to propagate in certain directions through the structures; hence, they are diffracted and reflected, giving rise to the myriad of brilliant colors we observe in many insects.

For example, the bright, gem-like reflecting exoskeleton of many species of beetles, especially Coleoptera and Curculionidae, is not a result of the presence of pigments but the presence of three-dimensional photonic structures, also referred to as *photonic crystals*. To list two particularly interesting beetles, the scales of *Pachyrrhynchus congestus*[13] weevils have a hexagonal close-packed arrangement of air-

spheres built into their exoskeleton, while the weevil *Lamprocyphus augustus*[14] produces its spectacular green coloration with a diamond-based air-cuticle lattice (i.e., face-centered cubic system).

In biological systems structural colors are used as a defense mechanism, mating signals, mimicry or as a camouflage tool to blend into their habitat. Many harmless organisms have evolved to mimic *aposematic*[*] species, for example, the black and yellow pattern on the hornet moth, *Aegeria apiformis*, contributes to its resemblance to a wasp or bee, but is not capable of stinging.[15] Animals such as the poison dart frog[16] native to Central and South America and cinnabar moth caterpillar[17] display aposematic patterns to prevent attack by warning potential predators. Not only animals but some plant species such as scarlet trumpet use their unique pigments also to attract pollinators.[18]

Millions of years after biology started to develop photonic structures and use structural colors, modern day research has embraced similar ideas to control light. While the motivation in biology and technology for developing photonic structures differs (the former uses these structures to create color effects for camouflage, mimicking, and signaling, whereas technological applications include coherent control of light, amplification, and guiding), structural features employed in both biology and technology are very similar.

In the late 1980s, the quest to find new ways to control light in materials led to the discovery of photonic band structure materials, also known as photonic crystals. In a photonic crystal (Figure 1.1), the periodic variation of dielectric constant leads to the appearance of the photonic band structures. These control how photons move thorough

[*] A*posematism*, a primary defense mechanism, is the use of bright conspicuous coloration or other perceivable characteristics by the prey animal to warn potential predators.

Figure 1.1 Schematics of photonic crystals. Different colors represent different dielectric materials[19].

the crystal, in a similar way as the periodic arrangement of ions on a lattice gives rise to the electronic bands which controls the motion of charge carriers in semiconductors.[20] Photons propagate through the structure depending on their wavelength. The group of allowed modes, the wavelengths of light that are allowed to propagate, forms bands. In several recent studies, several dielectric structures have been predicted (and some also experimentally confirmed) to show a photonic band-gap, a range of frequencies for which no electromagnetic modes are classically allowed to propagate through the material.[21, 22] Such photonic crystals exhibit a variety of distinct optical phenomena such as suppression of spontaneous emission[20], omnidirectional mirrors, low-loss waveguiding and quantum information processing.[23] More recent studies show that the position of a photonic band-gap can be controlled by modifying the refractive index or the periodicity of the photonic crystal structure.[24]

1.2 History of Photonic Crystals

In 1887, Lord Rayleigh studied the electromagnetic wave propagation in periodic media and predicted that there exists a one-dimensional photonic band-gap in one-dimensional photonic crystals.[25] These photonic crystals were studied in the form of periodically arranged multilayer dielectric slabs. About 100 years later, in 1987, two physicists Eli Yablonovitch and Sajeev John studied photonic crystals independently and published two milestone papers on high dimensional photonic crystals.[20, 26] Yablonovitch, an American physicist, engineered the photonic density of states, in order to control the spontaneous emission of materials embedded within the photonic crystal, while John used photonic crystals to affect the localization and control of light. They created a three-dimensional structure that exhibited a complete photonic band-gap.[21] In 1996, Thomas Krauss fabricated a two-dimensional photonic crystal structure with photonic band-gaps at low wavelengths (in the range 800-900nm).[27] This led to the novel phenomena in quantum optics and various technological applications. At the commercial level, photonic crystals have an excellent application in the form of photonic crystal fibers, developed by Philip St. J. Russell in 1998.[28]

1.3 Theoretical Background in Photonic Crystals

Photonic crystals are periodic dielectric structures with zero propagation of electromagnetic modes for the range of frequencies spanned by the band-gap.[20,26] Whenever electromagnetic radiation with a wavelength comparable to the lattice constant of the photonic crystal is incident upon the crystal, the electromagnetic waves are Bragg-scattered and undergo constructive or destructive interference. Thus, given the Bragg condition is satisfied, there exists a range of photon frequencies where no photons are

allowed to transmit through the material, called a photonic band-gap. A Brillouin zone exhibits all the wavevectors $\boldsymbol{k}$, which are Bragg-reflected by the crystal. Since the dispersion relation $\omega(\boldsymbol{k})$ is a periodic function of $\boldsymbol{k}$ outside the Brillouin zone, the calculations for the photonic band-gap are restricted only to the wavevectors $\boldsymbol{k}$ lying inside the irreducible Brillouin zone instead of considering all possible propagating directions in the photonic crystal. Hence, all the dispersion curves $\omega(\boldsymbol{k})$ of the photonic crystal can be represented by the wave vectors $\boldsymbol{k}$ present inside the irreducible Brillouin zone, which depends on the geometry of the lattice.

In 1928, in his doctoral thesis, Felix Bloch studied the propagation of electronic waves in three-dimensionally periodic media extending the Floquet's theorem in one dimension by Gaston Floquet (1883).[29] Bloch proved that waves in a periodic medium can propagate without getting scattered. He defined the Bloch wave function for a particle in a periodic environment by a periodic envelope function multiplied by a plane wave and predicted that the scattering of electrons in a conductor is due to the lattice defects and not from the periodic atoms.

In 1997, three physicists at the Massachusetts Institute of Technology, John D. Joannopoulos, Pierre R. Villeneuve and Shanhui Fan applied the same technique to electromagnetic waves. They showed that one can obtain an eigenvalue equation in only the magnetic field **H** by solving Maxwell's equations as an eigenvalue problem (analogous to the Schrödinger's equation) starting from the source-free (ρ = J = 0) Faraday's and Ampere's laws at a fixed frequency[30] (time dependence $e^{-i\omega t}$):

$$\boldsymbol{\nabla} \times \frac{1}{\varepsilon(\mathbf{r})} \boldsymbol{\nabla} \times \mathbf{H} = \left(\frac{\omega}{c}\right)^2 \mathbf{H} \tag{1.1}$$

where $\nabla \times \frac{1}{\varepsilon(\mathbf{r})} \nabla \times$ is the Hermitian eigen-operator, $\left(\frac{\omega}{c}\right)^2$ is the eigenvalue, c is the speed of light, and $\varepsilon(\mathbf{r})$, $\mathbf{r} = (x, y, z)$, is the dielectric function. The periodic dielectric function corresponding to a photonic crystal is given by $\varepsilon(\mathbf{r}) = \varepsilon(\mathbf{r} + \mathbf{R}_i)$, where $\mathbf{R}_i$ are the primitive lattice vectors (i = 1, 2, 3 for a crystal periodic in one, two, or three dimensions, respectively).

According to the Bloch-Floquet theorem for periodic eigenproblems, the solutions to Eq. (1.1) can be chosen in the form $\mathbf{H}(\mathbf{r}) = \boldsymbol{e}^{i\boldsymbol{k}\mathbf{r}}\mathbf{H}_{n,\boldsymbol{k}}(\mathbf{r})$ with eigenvalues $\omega_n(\boldsymbol{k})$ representing the frequencies of allowed harmonic modes, where $\boldsymbol{k}$ is a Bloch wave function and $\mathbf{H}_{n,\boldsymbol{k}}$ is a periodic function satisfying the following equation[30]:

$$(\nabla + i\boldsymbol{k}) \times \frac{1}{\varepsilon(\mathbf{r})} (\nabla + i\boldsymbol{k}) \times \mathbf{H}_{n,\boldsymbol{k}} = \left(\frac{\omega_n(\boldsymbol{k})}{c}\right)^2 \mathbf{H}_{n,\boldsymbol{k}} \tag{1.2}$$

This equation (1.2) produces a different Hermitian eigenproblem over the primitive cell of the lattice at each Bloch wavevector $\boldsymbol{k}$.

If the structure is periodic in all directions, this leads to discrete eigenvalues $\omega_n(\boldsymbol{k})$ which are continuous functions of $\boldsymbol{k}$ with n = 1, 2, ⋯. The band structure or dispersion diagram can be obtained plotting these eigenvalues $\omega_n(\boldsymbol{k})$ versus the Bloch wavevector $\boldsymbol{k}$; where both ω and $\boldsymbol{k}$ are conserved quantities. The eigensolutions are periodic functions of the wavevector $\boldsymbol{k}$. By solving equation (1.1) for the first few eigenvalues over the principle directions in the photonic crystal, the allowed frequencies within the crystal can be evaluated and summarized in a photonic band diagram.

A complete photonic band-gap can be defined as the range of frequencies ω for which there are no propagating solutions of Maxwell's equations (1.2) for any $\boldsymbol{k}$, with propagating states above and below the band-gap. The maxima and the minima of the

function $\omega(\boldsymbol{k})$ occur at the irreducible Brillouin zone edges, which are obtained by eliminating the redundant regions inside the first Brillouin zone using the reflection symmetries.

The harmonic modes can be found by using the variational principle. The eigenvalues minimize a variational problem in terms of the periodic electric field envelope $\boldsymbol{E}_{n,\boldsymbol{k}}$:

$$\omega^2{}_{n,\boldsymbol{k}} = \min_{\mathbf{E}_{n,\boldsymbol{k}}} \frac{\int \left|(\nabla \times i\boldsymbol{k}) \times \mathbf{E}_{n,\boldsymbol{k}}\right|^2}{\int \varepsilon \left|\mathbf{E}_{n,\boldsymbol{k}}\right|^2} \, c^2 \tag{1.3}$$

where the numerator and the denominator correspond to the kinetic and the potential energy, respectively. By symmetry, the harmonic modes of the propagating electromagnetic field can be divided into two polarizations, transverse-magnetic (TM) and transverse-electric (TE), each with its own photonic band structure (dispersion diagram).

The higher bands are constrained to be orthogonal to the lower bands for $m < n$.

$$\int \mathbf{H}^*_{m,\boldsymbol{k}} \mathbf{H}_{n,\boldsymbol{k}} = \int \varepsilon \mathbf{E}^*_{m,\boldsymbol{k}} \mathbf{E}_{n,\boldsymbol{k}} = 0 \tag{1.4}$$

At each $\boldsymbol{k}$, there exists a gap between the lower dielectric bands concentrated in the high dielectric region and the upper air bands that are concentrated in the low dielectric. The dielectric/air bands in the photonic crystal are similar to the valence/conduction bands in a semiconductor. In order for a complete band-gap to arise in two or three dimensions, the band gap corresponding to each $\boldsymbol{k}$ point should overlap, which implies a minimum ε contrast.

The existence of a photonic band-gap depends on the two polarizations (TM and

TE) of the electromagnetic radiation (classically referred to as the *s* and *p* polarizations, respectively), and the boundary conditions at the material interface.[31] An omnidirectional band-gap is achieved only with a three-dimensional photonic crystal when the incident electromagnetic radiation with a frequency in the photonic gap region is reflected from the crystal for all angles of incidence and all polarizations.[31] A three-dimensional photonic structure is a face-centered cubic (*fcc*) lattice of air cylinders in a high-dielectric matrix. The first Brillouin zone of such a crystal is a truncated octahedron with an irreducible Brillouin zone defined by vertices Γ, L, U, X, W and K with origin at the point $\Gamma = (0, 0, 0)$, as shown in Figure 1.2. The dispersion curves of the photonic band diagram can be analyzed by considering the wave vectors $\boldsymbol{k}$, originating from the Γ-point, which describe the edge of the polyhedron-shaped irreducible Brillouin zone.

The existence of a complete band-gap depends on the ratio of the dielectric constants, the volume fraction of the dielectric material, and the geometry of the three-dimensional periodic structure.[32]

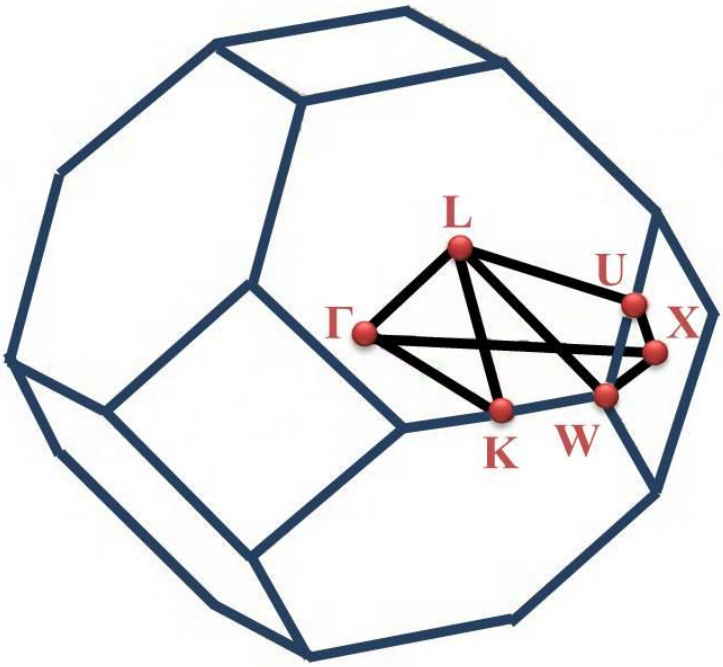

Figure 1.2 Brillouin zones of a face-centered cubic crystal: Truncated octahedron is the first Brillouin zone, and the polyhedron with vertices Γ, L, U, X, W and K is the irreducible Brillouin zone.

CHAPTER 2

BIOLOGICAL PHOTONIC CRYSTALS

2.1 Introduction

A delicate interplay of incident light with the intricate patterns of the weevil *Eupholus chevrolati's* exoskeleton scales produces a large number of sparkling colors and vivid hues. The reason for this beetle's coloration lies in a hierarchical photonic structure system covering its exoskeleton, consisting of multicolored micron-sized domains of three-dimensional photonic crystals. A striking feature of *E. chevrolati's* appearance is that while it has a macroscopic uniform yellowish-green coloration, this 'uniform' color is the result of multicolored (from blue to green, yellow and red) micrometer-sized domains. Figure 2.1 shows various scales with differently colored domains. To unravel the mystery behind this optical effect, the photonic structure within each micrometer scale and sub-micrometer domain was investigated using the valuable characterization techniques such as optical microscopy, scanning electron microscopy and focused ion beam microscopy. We modeled the three-dimensional architecture of the photonic crystals from the SEM images, studied the origin and properties of the resulting photonic band structure, computed the photonic band diagram using MIT's photonic bands (MPB) software package,[33] and compared the calculations to experimental high-resolution optical spectroscopy studies.

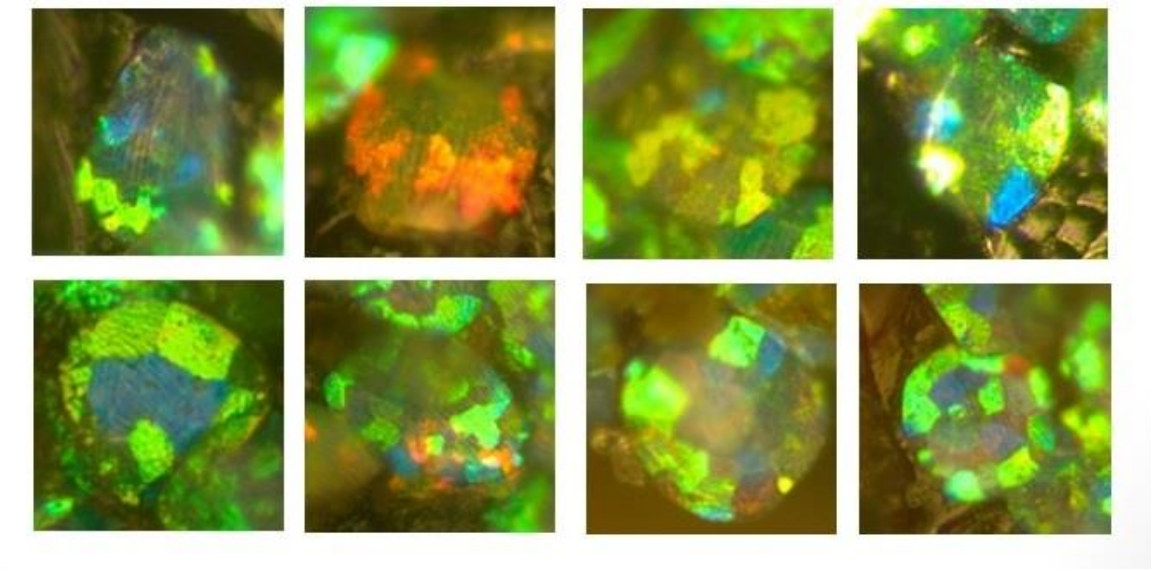

Figure 2.1 Optical microscopy images of iridescent scales of the weevil *E. chevrolati*, demonstrating differently colored domains.

2.2 Materials and Characterization

In this section we introduce the experimental techniques used in this thesis including the optical and structural characterization of biological photonic structures, and calculation of photonic band diagrams for the structure present inside the exoskeleton of the weevil *E. chevrolati*.

2.2.1 Optical Characterization

One of the most common methods to experimentally characterize a photonic crystal is optical reflectance measurement. The range of wavelengths of electromagnetic waves, which are forbidden to propagate in a certain direction through the photonic crystal, are totally reflected, determining the photonic stop-gap (a directional band-gap).[20,26] Experimentally, this is characterized by the presence of an inhibited

transmission with an associated reflection peak at the characteristic frequency/wavelength range.[20]

The yellowish-green iridescence of the scales found on the exoskeleton of the weevil *E. chevrolati* was investigated by the optical microscopy technique. The optical spectra were taken at normal incidence with an Ocean Optics USB4000 spectrometer fiber coupled to a Nikon EclipseME600 microscope. White light from a ThorLabs OSL1 Fiber Illuminator was focused onto the specimen using a $20\times$ objective lens with numerical aperture (NA) of 0.46. The experimental setup is shown in Figure 2.2. The reflection measurement was normalized to a high reflectance broadband mirror as 100%. A pinhole with 0.5 mm aperture was inserted into the image plane of the optical path to isolate small areas of the exoskeleton (as small as ~5 μm in diameter). The exoskeleton of the weevil was cut into small sections (~ 1 mm), and reflectance spectra from the individual domains in the scales were measured and analyzed.

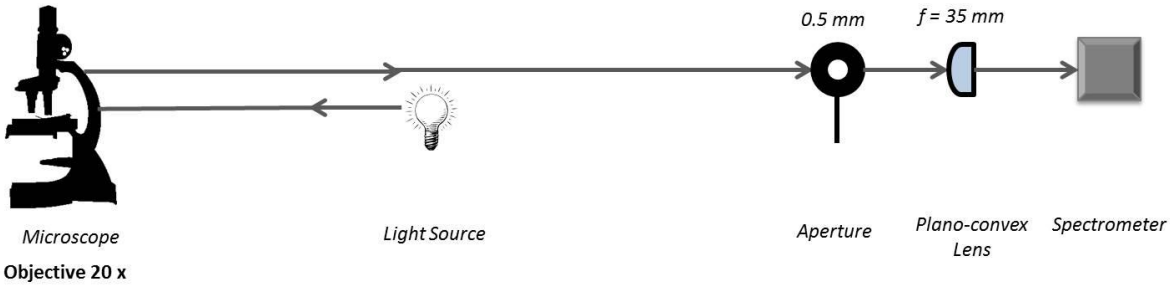

Figure 2.2 Experimental set up for optical characterization.

2.2.2 Structural Characterization

The photonic structure inside of iridescent scales of the weevil *E. chevrolati* was examined by high-resolution structural analysis based on scanning electron microscopy (SEM) combined with focused ion beam (FIB) milling. SEM and FIB were conducted using a FEI NanoNova 630 microscope and a FEI Helios NanoLab 650 system, respectively. The structural characterization of the weevil scales was executed by first gently scraping a few scales from the exoskeleton of the weevil onto a microscope slide using a razor blade. The scales were then transferred onto the conductive carbon adhesive tab SEM sample holder. The scale was carefully oriented vertical using a scalpel. By orienting the scale vertical and adjusting the angles of rotation and tilt of the FIB stage, a layer of thickness ~0.7 μm was removed from the top surface of the scale using FIB with ion beam current of 430 pA and 30 kV accelerating voltage. The subsurface internal photonic structure thus exposed, provided us with a view of the all domains within a single scale. High resolution images of the structure of each domain were taken by FEI NanoNova SEM. Since the nonconductive specimens tend to charge when scanned by the electron beam using high vacuum mode, an ultrathin layer of gold was deposited on the top surface of the scale by sputter coating before SEM imaging.

The SEM images were later processed using the image-processing software ImageJ. The structural parameters were obtained from analyzing the structural features of the cross-sectional SEM images of each domain. Using the quantitative information thus obtained, a face-centered cubic lattice-based[30] three-dimensional photonic structure of the domains was created. The two-dimensional cross-sectional projections of the structure model obtained by making oblique cuts through the volume were compared with the

SEM images taken of each domain on the weevil scale.

2.3 Results and Discussion

In this section we present our detailed analysis of the observed wide range of chromatic effects in the weevil *E. chevrolati* (dried specimen) from spectral reflection studies and anatomy of the weevil by implementation of high-resolution imaging techniques.

2.3.1. Micropixelation and Color Mixing

To understand the origin of the angle-independent homogeneous yellowish-green color in the studied weevil (see Figure 2.3 (a)), we employed the routinely used characterization technique, optical reflection spectroscopy.

A typical optical reflectance spectrum of large sections of the weevil (100's of scales) is given in Figure 2.4. It displays a broad reflection peak centered at ~540 nm consistent with the weevil's macroscopic yellowish-green appearance. The large number of spectral features of the reflection peak indicates that this reflection spectrum is a mixture of many individual reflection peaks originated from different scales. To test this hypothesis we collected reflectance spectra from individual scales of the weevil's exoskeleton. These measurements revealed that reflection properties differ strongly from scale to scale. This finding is summarized in Figure 2.5, which compares the envelope reflection peak of a large area of the weevil's surface with the wavelength position of the peak maxima of 17 individual scales. It is evident that the overall reflectance behavior of this weevil is the result of color mixing at the micrometer-scale.

Moreover, analysis of the optical reflection micrographs of individual scales

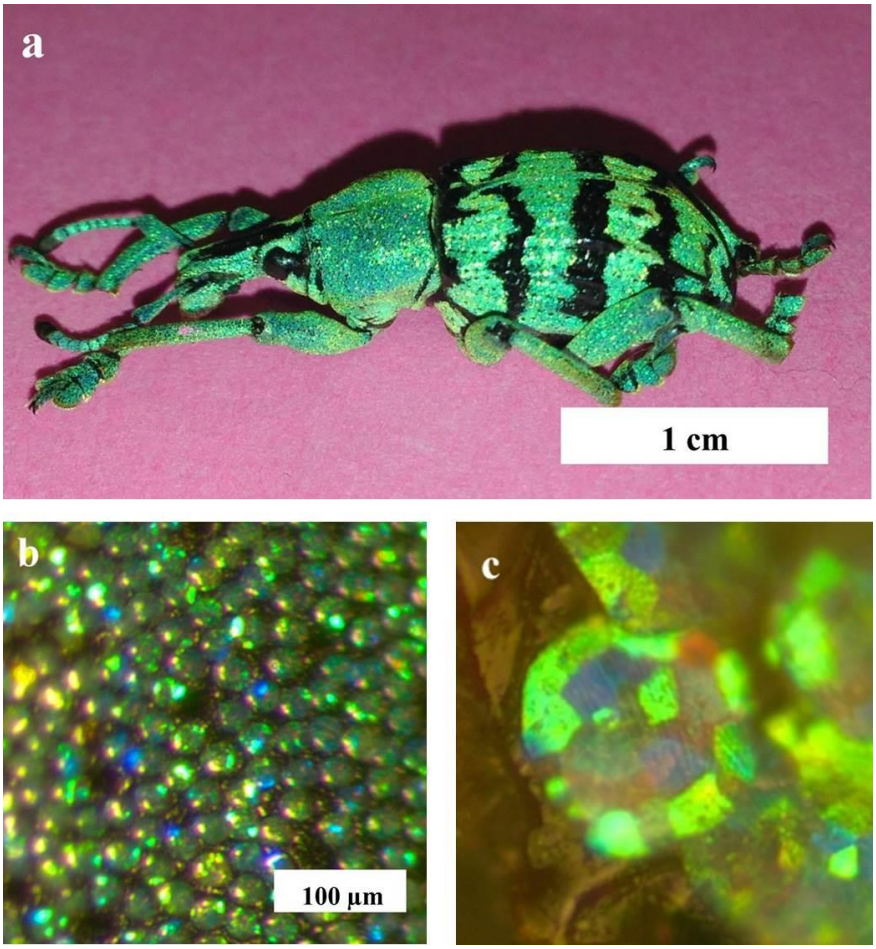

Figure 2.3 Multiple levels of the weevil *E. chevrolati's* hierarchical structure: exoskeleton, scales and domains. **(a)** Photograph of the weevil *E. chevrolati*. **(b)** Optical microscopy image of iridescent scales attached to the exoskeleton of *E. chevrolati* under white light illumination. **(c)** Magnified optical microscopy image of individual scales showing differently-colored domains.

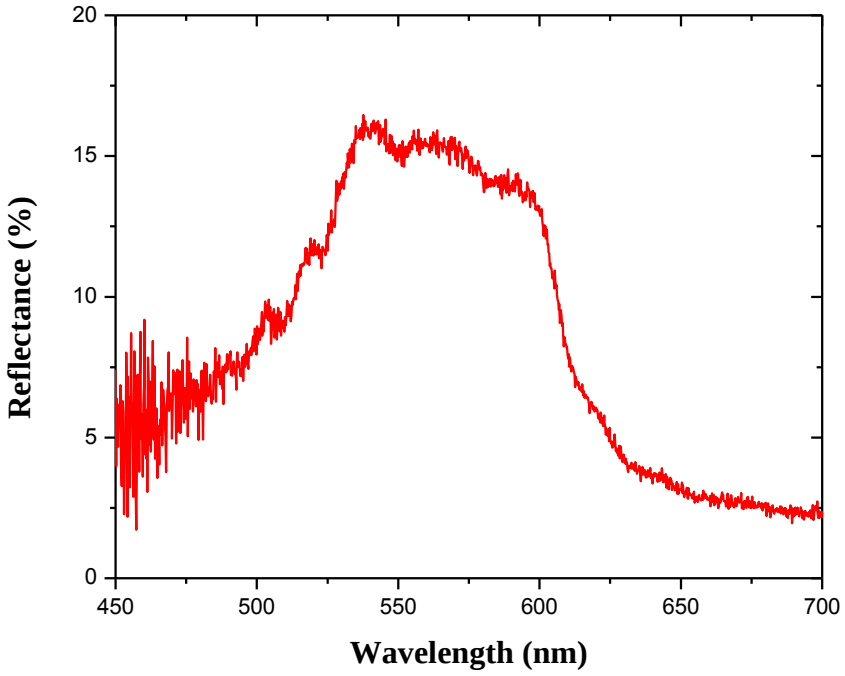

Figure 2.4 Optical reflectance spectrum for the weevil *E. chevrolati*.

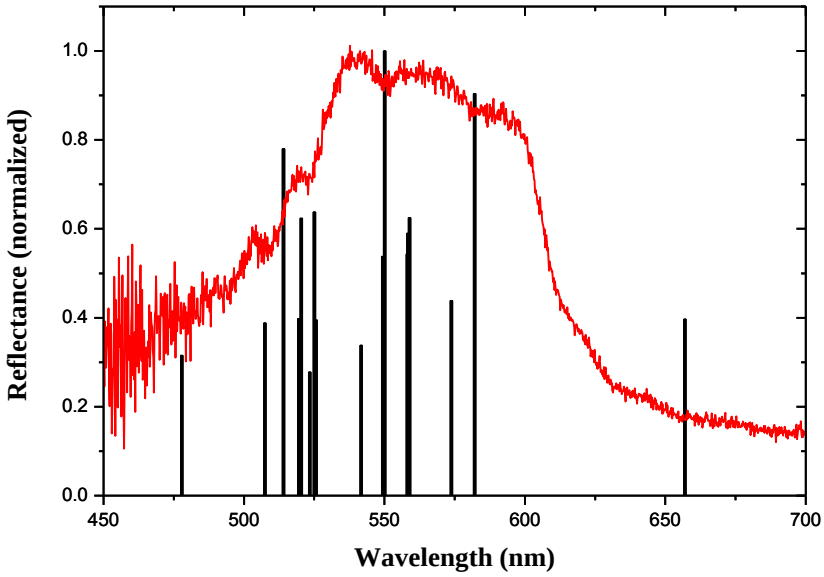

Figure 2.5 Reflectance spectra for *E. chevrolati* as an envelope to the peak reflection from individual scales.

(Figure 2.1) shows that color-mixing occurs at even smaller length scales, namely between individual domains within a single scale. We therefore optimized our micro-reflectance spectroscopy set-up to allow us to measure spectra of individual scale domains (around 2-10 μm in size). The resulting spectra of five domains of a particular scale are presented in Figure 2.6 (together with the optical micrograph) and demonstrate the distinct reflection properties of individual domains.

These high spatial-resolution measurements were repeated for a total of 80 different domains within different scales from multiple areas of the weevil's exoskeleton. The results are summarized in Figure 2.7. A comparison of all the peak maxima wavelength positions with the envelope spectrum demonstrates excellent agreement, confirming the hypothesis of *additive color-mixing of pixel-like domains* as the origin behind the yellowish-green coloration of the weevil *E. chevrolati*. In addition, the generated mixed color depends on the luminance levels of all individual pixelated color domains. A full range of colors perceivable by a human observer can be produced from the colored domains and an adjustment of their luminance levels. To further analyze this color-mixing phenomenon and find an explanation for the weevil's angle-independent coloration with a dull, low saturated hue, the concept of color theory has been applied and will be discussed in detail in Section 3.2 of Chapter 3.

2.3.2 SEM Structural Studies of Individual Scales and Domains

To examine the origin of the different coloration of individual domains the structural properties of scales and domains were investigated by a combined SEM imaging and FIB milling study. For this, the exoskeleton of a dead, dried weevil specimen was dissected into small pieces and individual scales, and mounted onto SEM

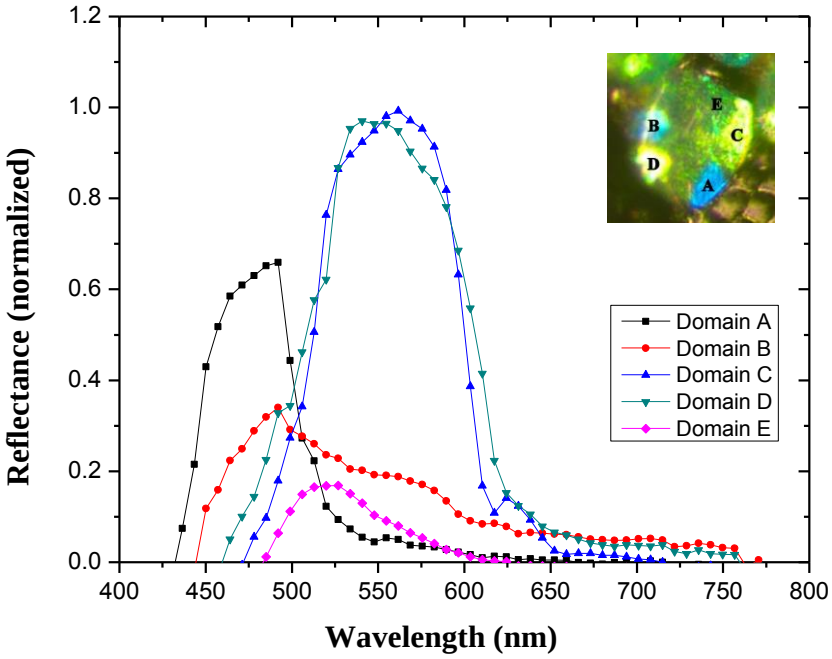

Figure 2.6 Optical reflectance spectra of individual domains on a single scale shown as an inset.

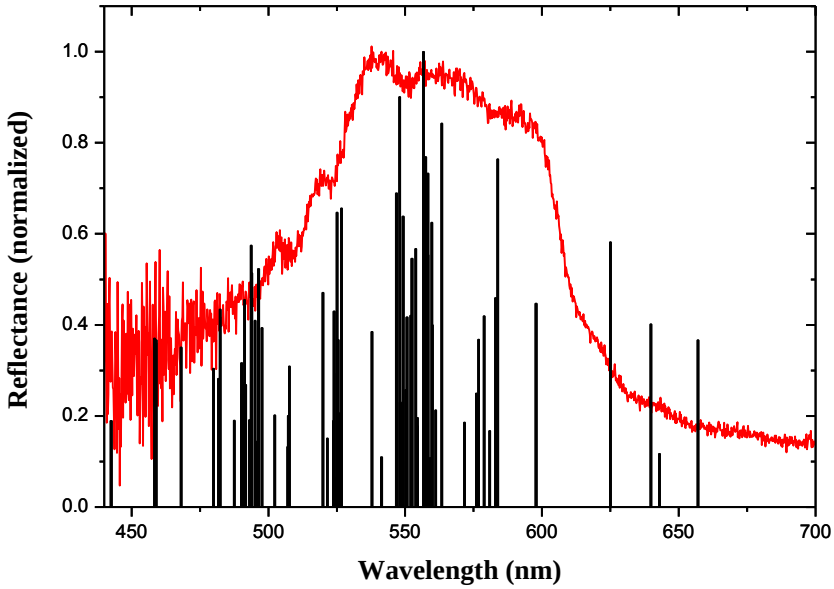

Figure 2.7 Reflectance spectra for *E. chevrolati* as an envelope to the peak reflection from individual domains.

sample holders. The FIB milling technique was then used to cut scales and expose the interior cuticle structure. An example of a random cross-sectional cut is presented in Figure 2.8.

In a single scale, differently-colored domains are horizontally stacked and spread across its entire volume, and the structure of each domain extends from the top to the bottom surface (~5 μm) of the scale. To investigate the structural arrangement of a domain generating a specific wavelength, the entire scale was first mapped with all the existing domains on its CCD image (see Figure 2.9 (a)), then, as mentioned in Section 2.2.2, the outermost protective layer of the vertically-oriented scale, as shown in Figure 2.9 (c), was removed from the top using the FIB technique. It was observed that the use of an ion beam on the horizontal scale on the SEM stub resulted in an uneven top surface, as can be seen in Figure 2.10. However, after the alignment of the *xz*-plane of the scale with the ion beam direction and limiting the ion beam current to 430 pA (higher values of current rendered the soft chitin structure to melt as can be seen in Figure 2.11) we were provided with a clean-cut top surface with clearly-defined domain boundaries as shown in Figure 2.9 (d).

The high-resolution image of the scale's top surface, thus obtained, was matched with its CCD image, and each individual domain was depicted in its SEM image (Figure 2.9 (d)). To study the structural characteristics of each domain, individual domains were then imaged using SEM, as shown in Figure 2.12 and 2.13.

Comparison of the exposed structural features of several different cross-sectional cuts with previous studies in the Bartl group on other types of weevils (in particular, *Lamprocyphus augustus*) revealed strong similarities. More detailed structural

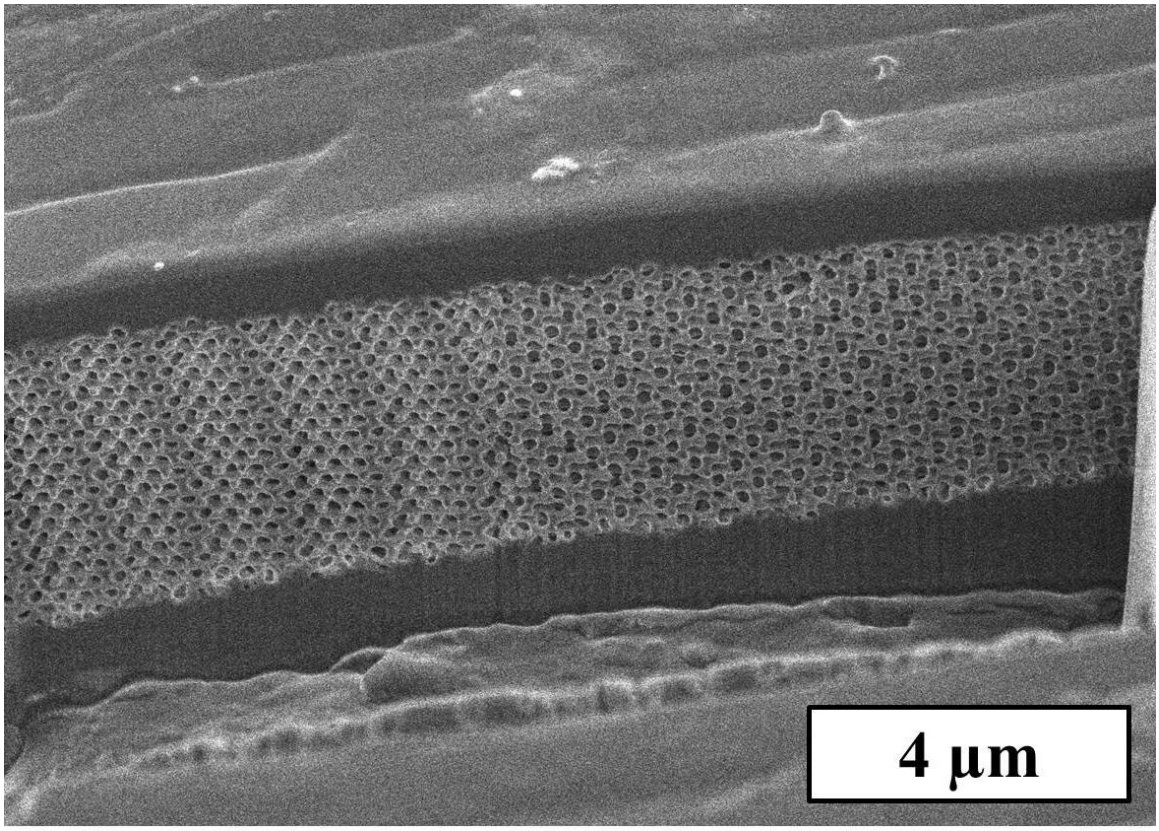

Figure 2.8 SEM of the exposed side surface of the sample scale.

examination confirmed a similar structure of ABC stacked layers of air cylinders arranged in a face-centered-cubic (fcc) lattice in a surrounding dielectric matrix made of chitin (a polysaccharide-based biopolymer with refractive index of 1.53).

Quantitative analysis yielded a height and radius of the air cylinders of 300 ± 25 nm and 71 ± 7 nm, respectively. The lattice constant, *a*, was found to vary in the range between 360 and 400 nm.

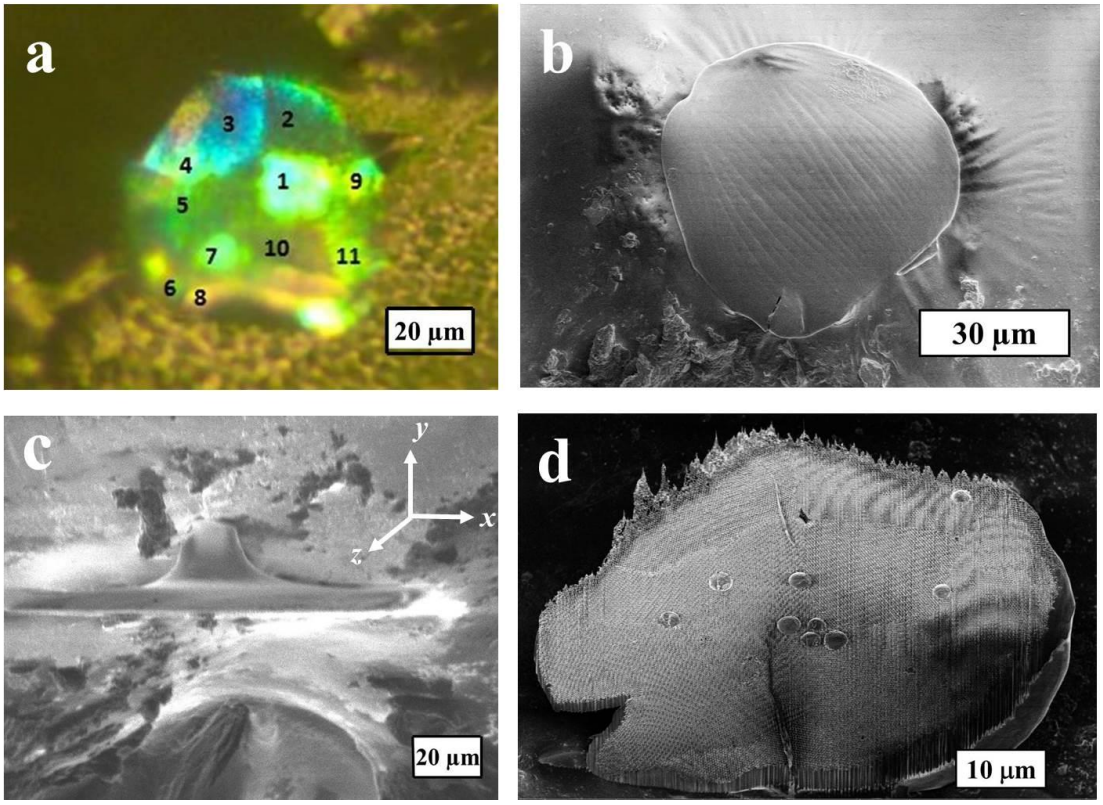

Figure 2.9 Images of the sample scale. **(a)** CCD camera image. **(b)** SEM image of the horizontal scale. **(c)** Ion beam image of the scale oriented in the *xz*-direction. **(d)** SEM image of the exposed top surface of the vertically-oriented scale.

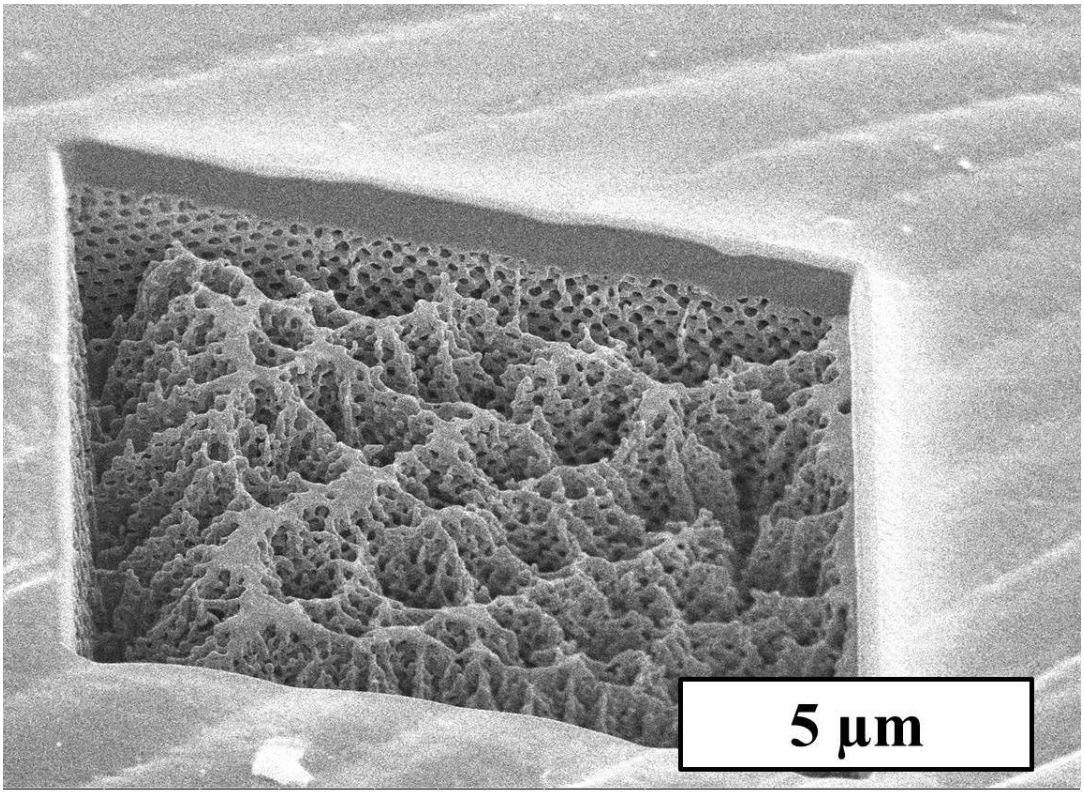

Figure 2.10 SEM image of the horizontal scale's top surface after FIB milling.

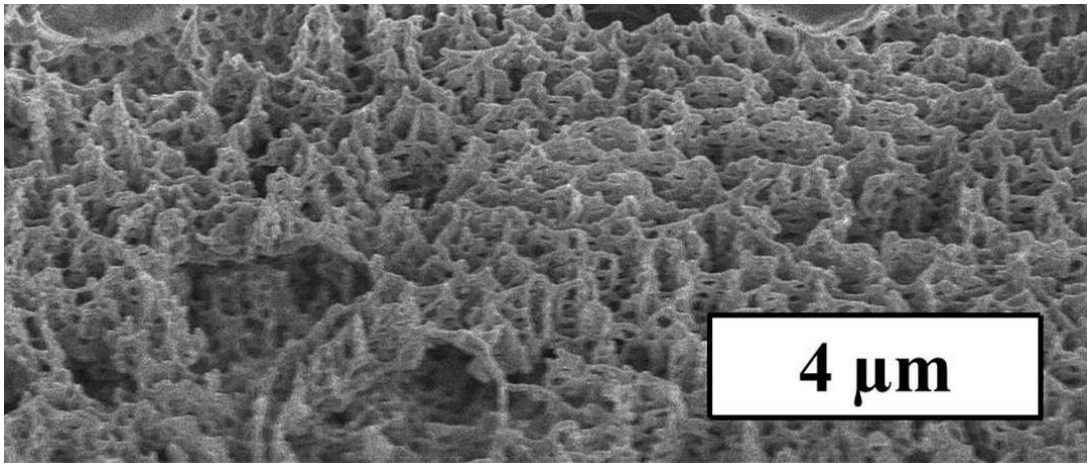

Figure 2.11 SEM image of the melted internal structure when an ion beam current > 430 pA was used.

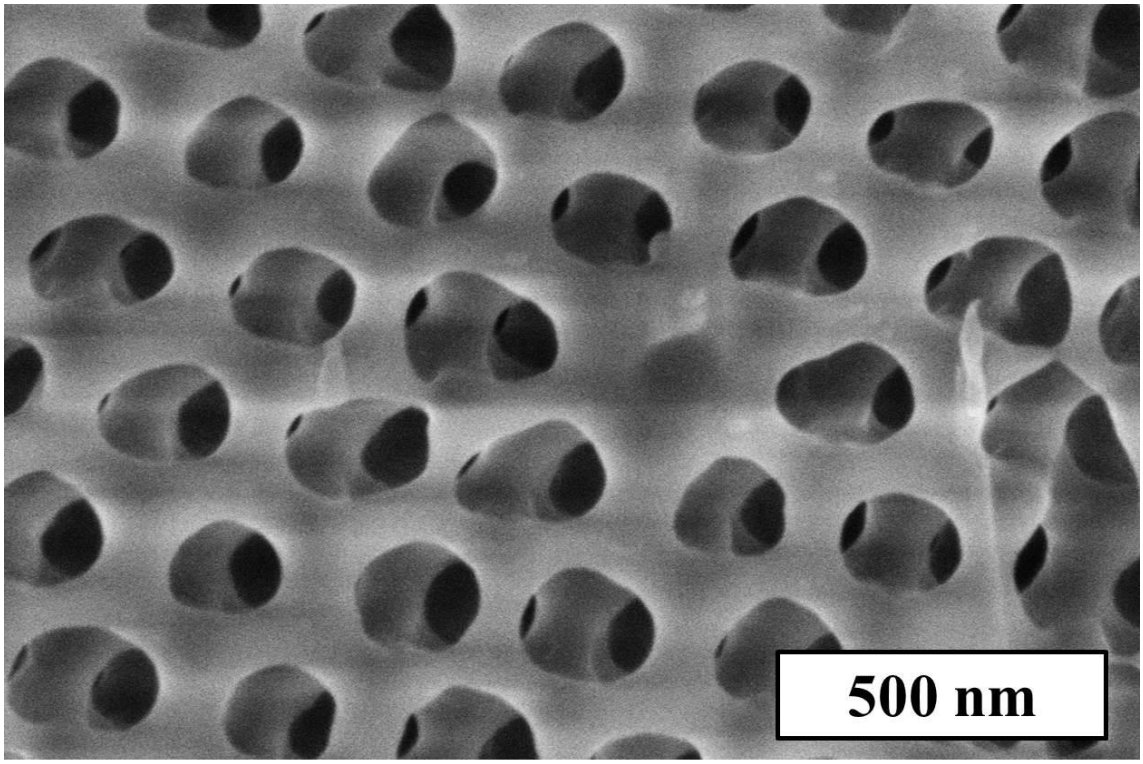

Figure 2.12 SEM image of a single domain.

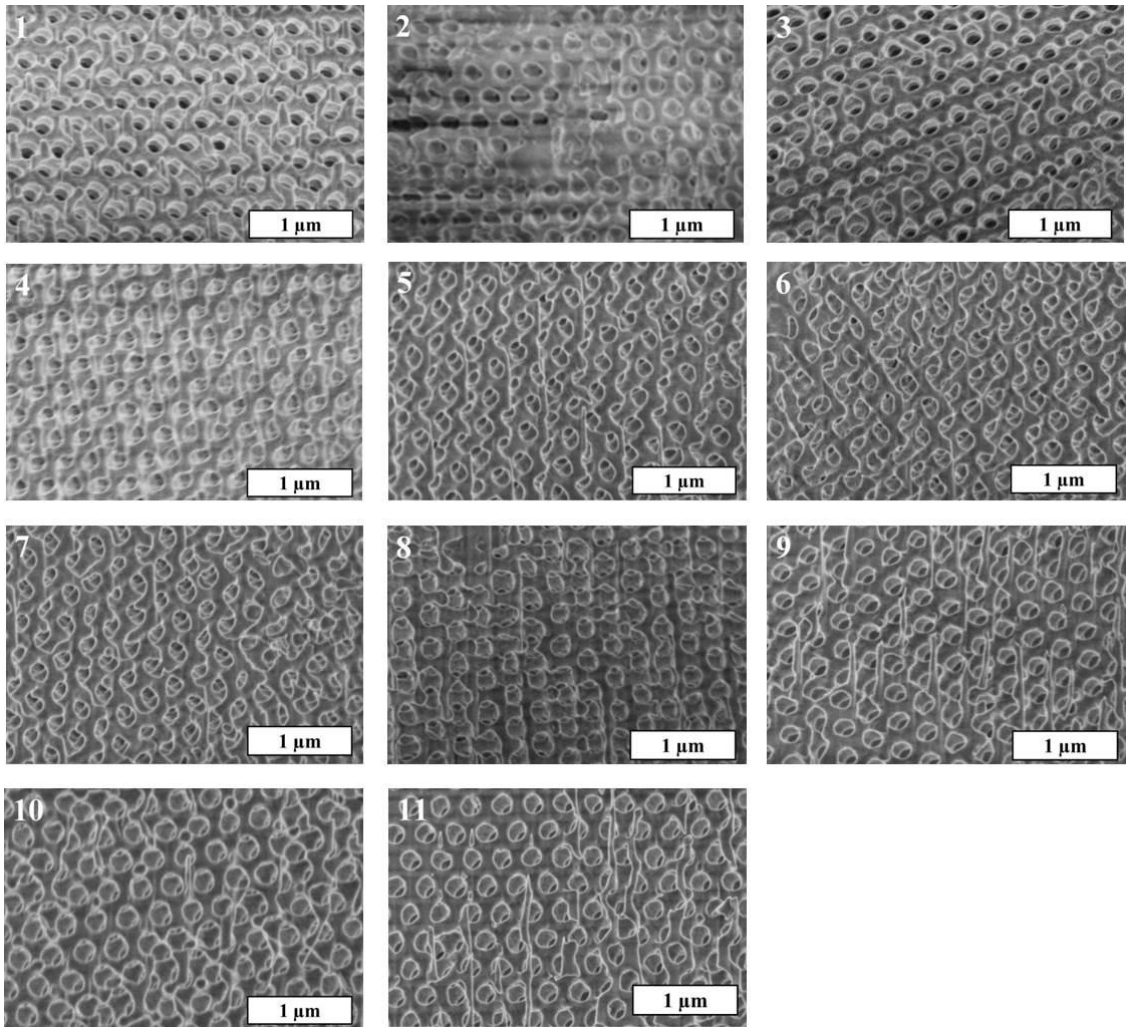

Figure 2.13 Cross-sectional scanning electron microscopy images of the individual domains on the sample scale.

2.3.3. Band Structure Studies and Comparison to Optical Properties

Due to the presence of additional symmetries of the face-centered cubic lattice structure, the energy bands are invariant under spatial reflection symmetry, the wavevectors describing an irreducible Brillouin zone of the lattice are sufficient to define the photonic band structure. The maxima and minima of the eigenvalues occur at the edges of irreducible Brillouin zone defined by the vertices Γ, L, U, X, W and K. The photonic stop-bands are the gaps between any two consecutive allowed modes in the photonic band diagram. As described in Section 1.3 of Chapter 1, electromagnetic modes inside a photonic crystal structure can be calculated by finding the eigenvalues of the modified Hermitian eigenproblem (the frequencies of allowed harmonic modes). MIT's photonic bands (MPB) software, designed for the study of photonic band-gap materials, computes the definite-frequency harmonic modes of Maxwell's equations in periodic dielectric structures and dispersion relations.[33] Figure 2.14 presents a photonic band diagram of the weevil *E. chevrolati's* photonic crystal structure with a face-centered cubic arranged air-cylinder lattice, calculated using the above mentioned photonic bands software.[†]

A three-dimensional model of the photonic structure inside the weevil was constructed using the evaluated structural parameters. Two-dimensional projections were obtained by making cuts along specific directions through the constructed volume of with face-centered cubic air-cylinder lattice structure (Figure 2.15).[†] These model crystal faces were compared to SEM images of the top-surface domains of individual scales (see Figure 2.13). A detailed comparison is shown in Figure 2.15, where the calculated

[†] The three-dimensional modeling and photonic band structure calculations (using the MIT photonic bands (MPB) software) were performed by Danielle Montanari, a graduate student in the Bartl group.

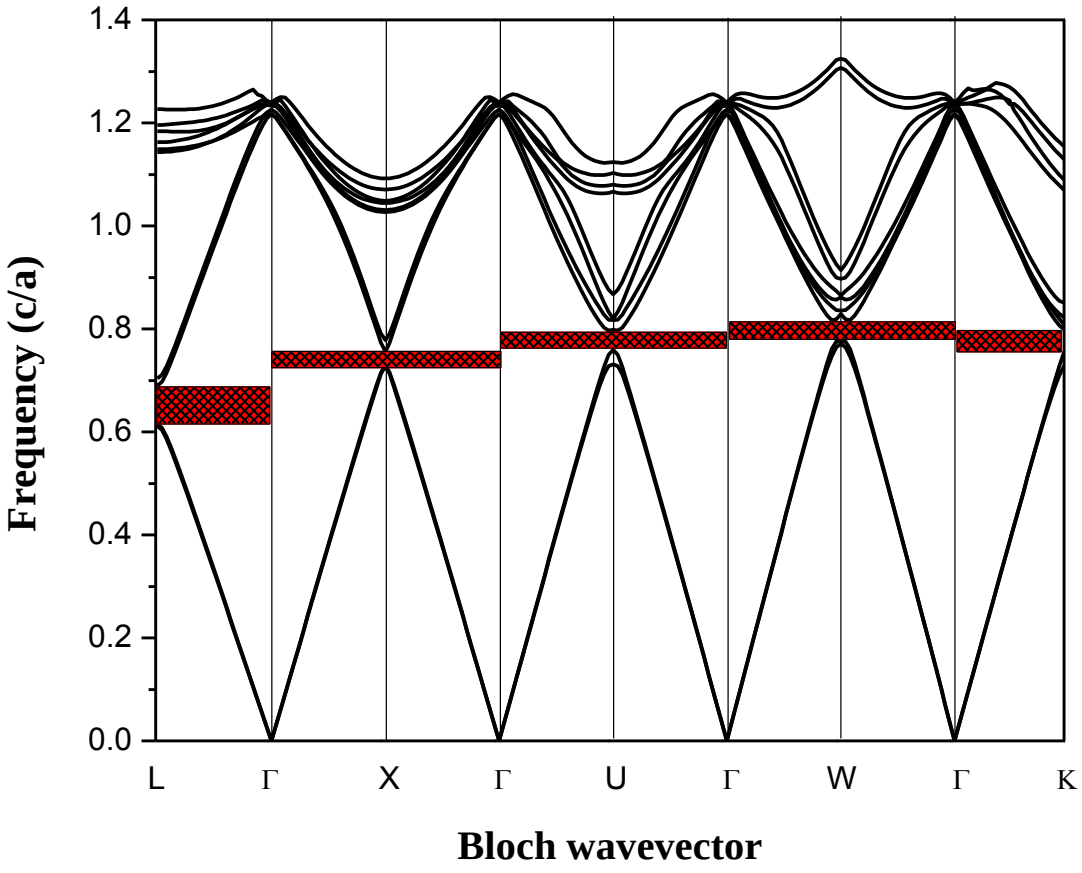

Figure 2.14 Photonic band diagram of the weevil *E. Chevrolati*.

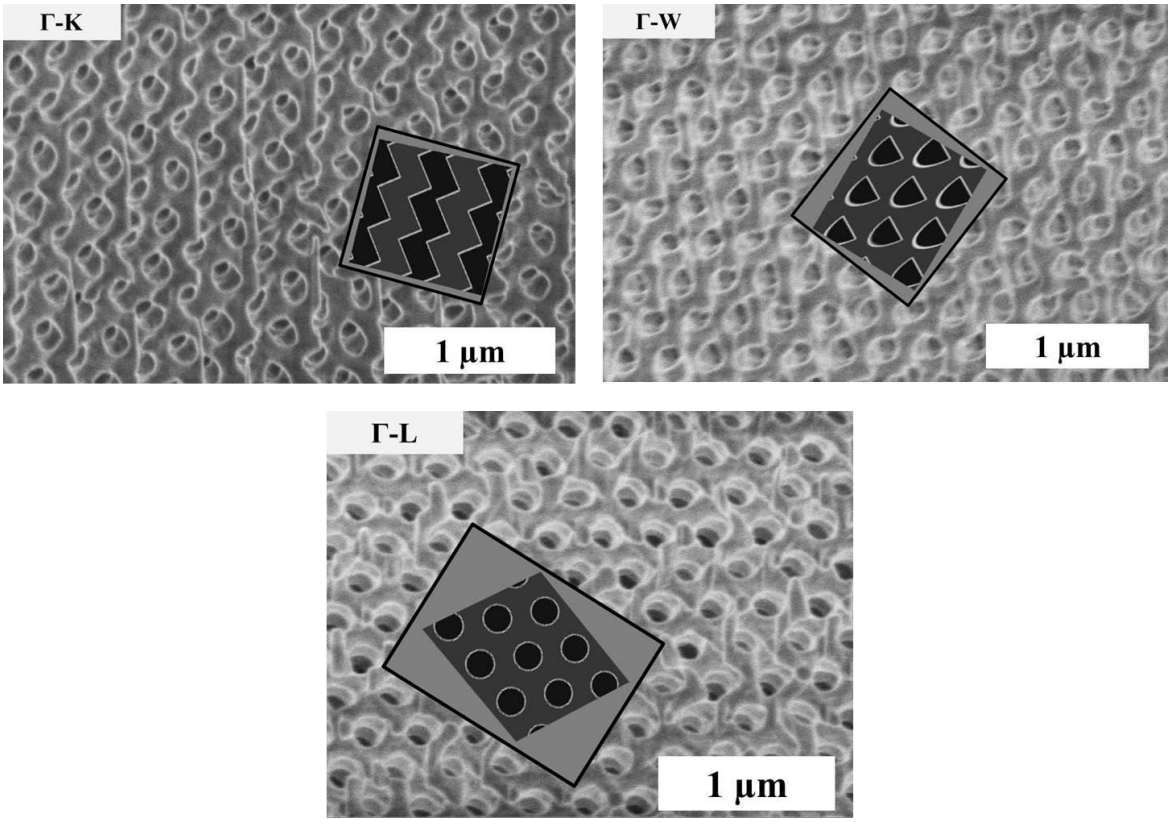

Figure 2.15 SEM images of individual single-crystalline domains oriented in Γ-L, Γ-K and Γ-W directions, with corresponding calculated dielectric function (insets in the figure).

dielectric function of model crystal faces in the directions Γ-L, Γ-K and Γ-W is superimposed over the SEM images of individual domains. It was found that the domains within the weevil scales do not follow specific main orientation. Each domain, based on a face-centered cubic lattice, within a scale is relatively oriented in a different direction resulting in only a certain range of wavelengths in the electromagnetic spectrum being reflected by it.

From the calculated frequency stop-band positions along main lattice directions, the corresponding wavelength ranges can be calculated from the mid-gap frequency values ω_o, by choosing structurally-relevant lattice constants. For the weevil photonic crystal structure, we determined the lattice constant to be in the range 360-400 nm. Thus, we calculated wavelength stop-gap positions for all main lattice directions for lattice constants of 360, 380 and 400 nm. Results are listed in Table 2.1. The architecture of the weevil *E. chevrolati's* exoskeleton consists of numerous scales, each scale with several domains and each domain built on the same set of building blocks, fcc cubic lattice structure, but different dimensions, more specifically, lattice constants. Depending on which facet of the domain's lattice structure is oriented in the direction of incident light, the structure forbids a range of wavelengths to propagate through the structure.

It can be concluded from the calculated values that each domain within the scale of the weevil *E. chevrolati* is capable of exhibiting a wide wavelength range within the visible part of the electromagnetic spectrum, with different directions spanning different ranges of wavelengths. As discussed earlier in Section 2.3.1, the yellowish-green coloration of the weevil results from the additive mixing of different colors reflected from different domains.

Table 2.1 Ranges of wavelength reflected by the photonic crystal structure with different lattice constants.

Directions	Mid-gap Frequency, ω_o (in units of c/a)	Wavelength Range (nm)		
		***a* = 360 nm**	***a* = 380 nm**	***a* = 400 nm**
Γ-L	0.66	511-585	540-618	568-650
Γ-X	0.74	476-493	503-521	529-548
Γ-U	0.78	451-474	476-500	501-526
Γ-W	0.80	441-462	465-487	490-513
Γ-K	0.79	444-470	469-496	494-522

The comparison of structural data, optical results and band structure calculations suggest that the wavelength ranges exhibited by the weevil were generated from the same crystal lattice structure but from differently oriented domains within a lattice constant range of 360-400 nm. For example, only the fcc lattice structure with lattice constant of 400 nm spans the red wavelength region in the Γ-L direction, whereas the green and blue wavelengths generate from at least one of the directions of the lattice built with a lattice constant ranging between 360 and 400 nm.

CHAPTER 3

MATHEMATICAL REPRESENTATION OF COLORS ON A COLOR SPACE

3.1 Introduction

As with all living organisms, animals evolve through thousands of generations, which has an enormous impact on their appearance and behavior. This process of change often results in accordance with their surroundings and the changes in their survival plan. Theories of evolution explain how various species are considered related to one another, like humans and apes, for example.

Colors existed long before the conception of life in Mother Nature. However, studies show that the same objects are perceived of as having different colors by different observers. Depending on the wavelength ranges in the electromagnetic spectrum required to reproduce their full visible spectrum, animals can be categorized into dichromats, trichromats, tetrachromats and pentachromats.[34] Humans and some other mammals have evolved trichromacy from early vertebrates.[35-38] It is estimated that trichromatic humans can discern up to 2.3 million different surface colors[39] and can distinguish wavelengths with a difference of as little as 0.25 nm[40]. Fish and birds are tetrachromats, that is, they have four types of cone cells and can detect energy of ultraviolet wavelength as well, whereas most other mammals such as the domestic dog and the ferret are dichromats.[41]

Colors help animals in identifying different objects.[40, 42]

Several ancient scientists including Aristotle were intrigued by the theory of color and the physical reason behind its existence. Isaac Newton[43, 44], Thomas Young, James Clerk Maxwell[45] and Lord Rayleigh, who are considered the giants in the field of physics, studied the nature of light and developed theories of color vision. In the early 18th century, Thomas Young presented his hypothesis on color perception in his lectures, stating that the presence of three kinds of nerve cells in the human eye results in the perception of different colors.[46]

Color vision is the ability to interpret the surrounding environment by processing the information contained in the visible light.[47] The color of an object is a result of the mixture of all wavelengths in the light leaving the surface of that object. This depends on the object's surface properties, its transmission properties and its emission properties. The viewer's perception of the color of the object depends on the ambient illumination and the characteristics of the perceiving eye and brain.

This chapter discusses the wide color ranges produced in the biological world, and the mathematical representation of perceived colors using color space diagrams. The color gamut can be specified in a color space such as the CIE *XYZ* color space, by calculating the tristimulus values of the three primaries: red, green and blue. The *XYZ* color system used here to produce the color gamut was developed by CIE (Commission Internationale de l'Eclairage) in 1931.[48, 49] The perceived color of an object is a visual effect of a specific color combination, which makes it of absolute importance to understand the behavior of color mixtures in case of light (additive) and chemical dyes (subtractive). Color theory provides a guidance to color mixing and perceived colors.

3.2 Color Theory

Colorimetry, the science of color, includes the perception of a color by the human brain and eye[50-52], the physics of electromagnetic radiation visible to the human eye, and the origin of color in materials.[53-55]

Colors can be broadly categorized in three ways: primary color, secondary color and tertiary color. Primary color cannot be produced from any combination of other colors, whereas secondary and tertiary colors can be created from a combination of two (primary) colors and three (primary or secondary) colors, respectively. Colors can be mixed together to produce other colors. This mixing of colors can be additive or subtractive.[56] The creation of color by mixing light of different colors is known as *additive color synthesis*. The light sensitive cones in the human eye detect these light signals and send them to the brain for processing this information. This biological process is explained in detail in the following section. The additive color process is observed in television screens where an image is generated by mixing small pixels of red, green and blue lights. The *subtractive color synthesis* is the creation of color by mixing different colors of dyes or paints. The *RGB color model* is an additive color model, whereas *CMYK color model*[57] is a subtractive color model (see Figure 3.1).

The concept of color can be divided into two parts: chromaticity and brightness. The *chromaticity* represents the quality of a color, and consists of two independent parameters, hue and saturation. *Brightness* is one of the three psychological dimensions of color perception which refers to the visual stimuli of the light intensity. *Hue* refers to the purity of a color, and is defined as the degree to which the stimulus can be related similar to the unique hues (red, green, yellow, and blue). *Saturation* represents the degree

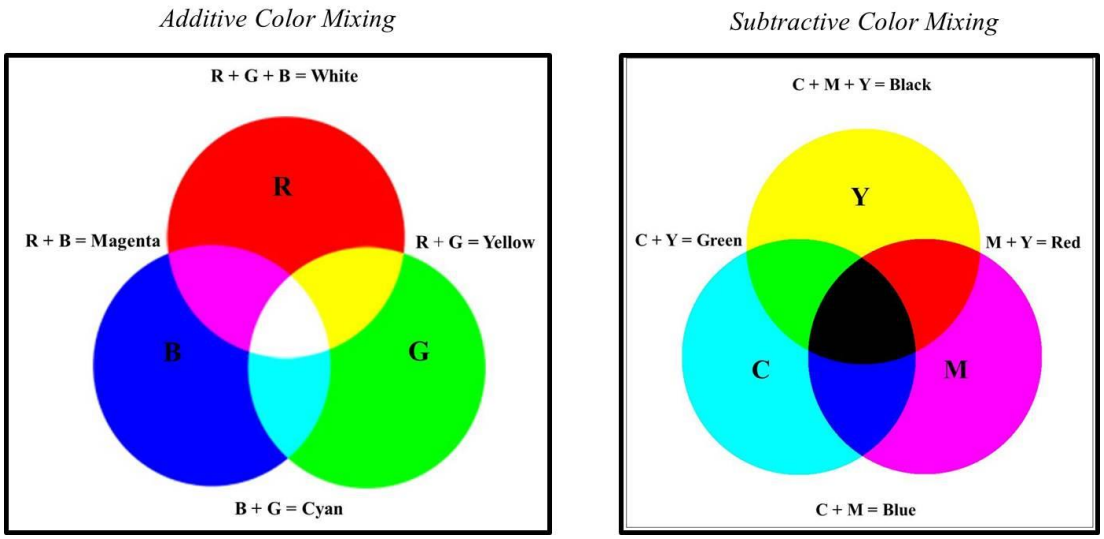

Figure 3.1 The color models: RGB (Additive) and CMYK (Subtractive).

by which a color differs from the gray of the same brightness.

An average human observer's response to a color can be described in terms of the amount of three primary colors (red, green, and blue) mixed together additively or subtractively to produce each wavelength of the visible range before it is perceived by the human eye.[58]

3.3 The Human Eye and Color Mixing

Human visual perception is based on the *color* and the *distance*[59]. Due to the spatial contrast sensitivity function of the human eye, the closer it is to an object, the finer detail it can resolve. At greater distances, the human eye tends to lose its *visual acuity*, which is a measure of *angular resolution*, specified in units of cycles per degree (CPD). The maximum resolution is 50 CPD for a human eye with excellent visual acuity.[60] The farther the eye moves away from an object (from the microscopic to the macroscopic view), the less resolved the features of the object become. This leads to the merging of

colors as the human brain tries to process the incoming information. Instead of seeing resolved spots/features, the human eye sees a total image of the object. In order to understand the response of a human observer to the colors found in their surroundings, it is of importance to understand the biological model of the human eye.

A human retina is a mosaic of two basic types of light sensors, also called photoreceptors: *cone cells* and *rod cells*, which are responsible for color and peripheral vision, respectively.[61] Each cell supplies information required by the visual system to create awareness of the surrounding environment through physical sensation. The resulting perception is known as eyesight or vision. *Visual acuity*, a property of the cone cells which are highly concentrated near the center of the retina called *fovea centralis*, is the ability to distinguish fine detail.[62] The lens of the human eye focusses the incoming light onto the photoreceptive cells of the retina, which is a part of the brain. The retinal neurons detect visible electromagnetic radiation and respond by producing neural impulses. Specifically, the photoreceptor proteins in the cells absorb the photons resulting in a change in the cell's membrane potential and produce electrical signals, which are processed by the brain to create an image of the visible surrounding environment. The color is detected by the cone cells which function best in the bright light. Although the rod cells are extremely sensitive to dim light, they cannot resolve sharp images or color. This explains why colors cannot be seen at night as only one photoreceptor cell is active.

Humans are *trichromats*.[47, 61, 63] Their retina consists of three different types of color receptors (called cone cells in vertebrates) with different absorption ranges of the electromagnetic spectrum, each containing a different photopigment. Young's idea of color vision was that it is a result of the three photoreceptors.[46] This was later expanded

by Helmholtz using color-matching experiments.[64] Each of the three types of cone cells in the human retina contains a different type of photosensitive pigment.[65] Each photopigment produces a neural response only when it is hit by a photon with a *specific* wavelength of light. The response curve is a function of wavelength and varies for each type of cone, giving the perception of any color sensation. The spectral sensitivity peaks of the three cone cells *S, M,* and *L* lie in the wavelength ranges 420-440 nm (*S,* short wavelength), 530-540 nm (*M,* medium wavelength) and 560-580 nm (*L,* long wavelength). They give three different signals based on the extent to which each cone cell is stimulated. These values of stimulations are called *tristimulus values*. The set of all possible tristimulus values determine the color space for a human observer.

3.4 Calculation of Chromaticity Coordinates

The *tristimulus values* depend on the observer's field of view due to the distribution of cone cells in the human eye, so CIE defined a standard observer, which represents the chromatic response of a human within a 2^0 arc of the *fovea centralis*‡.[66, 67] This particular angle was chosen by CIE because the *fovea*, a depression in the inner retinal surface, contains only the color-sensitive cone cells.[61] The chromatic response of an observer can be represented mathematically by the *color-matching functions* as shown in Figure 3.2, which when combined with the spectral power distribution of the incident light and the spectral reflectance leads to the tristimulus values of a color.

A color can be produced by additively mixing the red, green and blue color components of visible light. The primary colors are represented as *X* for red, *Y* for green and *Z* for blue.[6] The magnitude of the tristimulus values of a color gives the amount of

‡ A part of the human eye retina, where the density of cone-cells is the highest, responsible for sharp central vision.

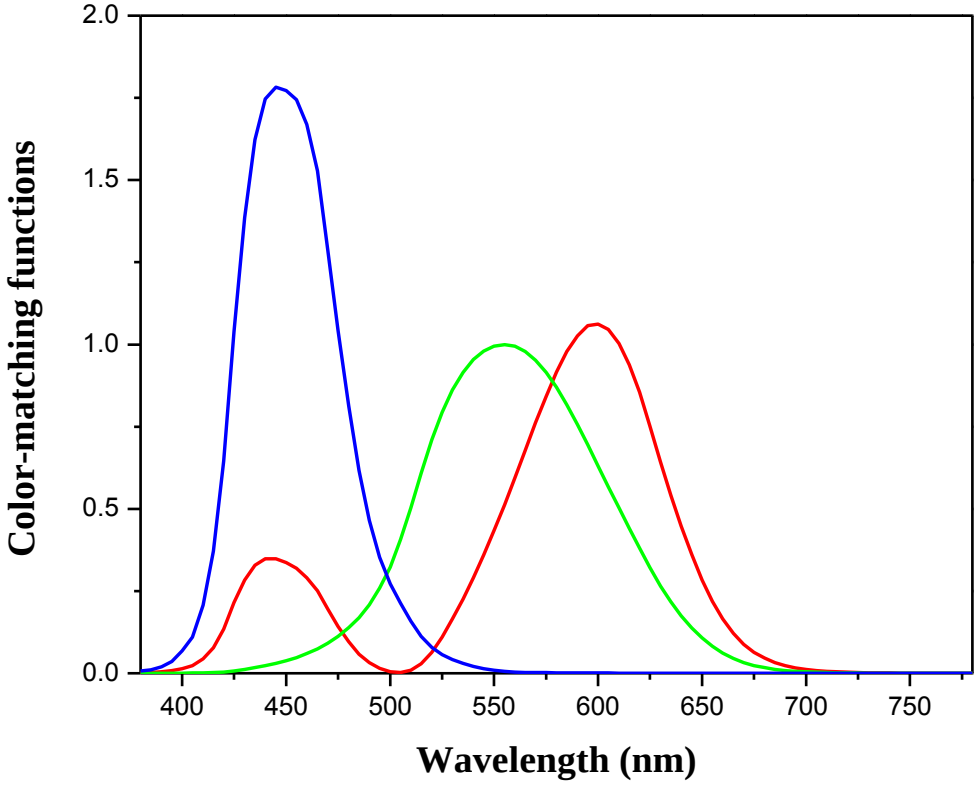

Figure 3.2 Color-matching functions of 1931 CIE standard 2° observer. Red, green and blue curves represent $\bar{x}$, $\bar{y}$ and $\bar{z}$, respectively.

each color required to be mixed additively in order to match a particular color. The chromaticity coordinates *x* and *y* can be computed by following the standard procedure given by CIE.[49]

The CIE *XYZ* color space, more specifically, CIE *xyY* color space is a horseshoe-shaped three-dimensional representation of all visible colors to a human observer, i.e., the gamut of all visible chromaticities where the solid outline represents the 'pure' hues that are perceivable to the human eye as shown in Figure 3.3. The parameter *Y* is a measure of brightness of a color, and the chromaticity of a color is defined by the parameters *x* and *y*.

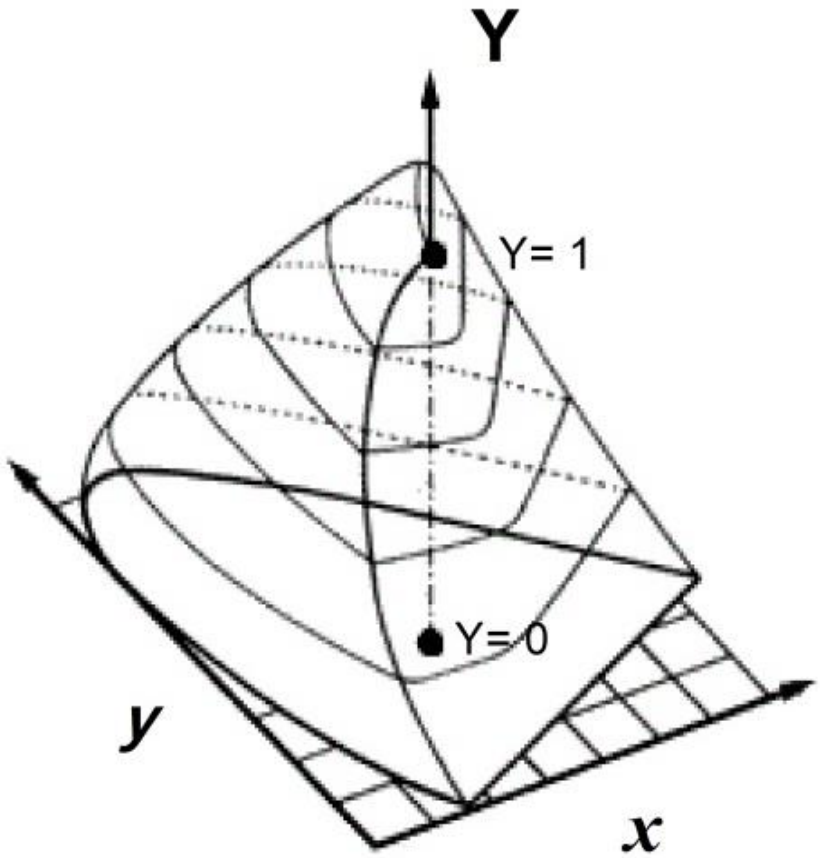

Figure 3.3 CIE 1931 *xyY* color space.

It is favorable to have a representation of 'pure' color in the absence of brightness.[68] The chromaticity coordinates can be conveniently represented using the CIE *XYZ* model. Hence, this specific color model was used to define the color gamut, for the biological photonic structures for a standard human observer.

The color perceived by a human observer can be represented numerically by the integral of the product of the spectral distribution of light source, spectral reflectance or transmittance of the object viewed and the color matching function of the standard observer over the visible range of the electromagnetic spectrum 380-780 nm.[69]

$$X = k \int_{780}^{380} R(\lambda) I(\lambda) \bar{x}(\lambda)\, \mathrm{d}\lambda$$

$$Y = k \int_{780}^{380} R(\lambda) I(\lambda) \bar{y}(\lambda)\, \mathrm{d}\lambda$$

$$Z = k \int_{780}^{380} R(\lambda) I(\lambda) \bar{z}(\lambda)\, \mathrm{d}\lambda$$

where $\bar{x}(\lambda)$, $\bar{y}(\lambda)$ and $\bar{z}(\lambda)$ are the color-matching functions[49, 70], $I(\lambda)$ is the spectral power distribution of the light source, $R(\lambda)$ is the spectral reflectance, $\mathrm{d}\lambda$ is the interval of wavelength and k is the normalization constant defined as $k = 100/\int I(\lambda)\bar{y}\, \mathrm{d}\lambda$.

The tristimulus values *X*, *Y* and *Z* thus obtained are normalized to obtain the three chromaticity coordinates *x*, *y* and *z* as below,

$$x = \frac{X}{X + Y + Z}$$

$$y = \frac{Y}{X + Y + Z}$$

$$z = \frac{Z}{X + Y + Z}$$

Only two chromaticity coordinates, *x* and *y*, are needed to define the color of an object since $x + y + z = 1$. The two coordinates *x* and *y* can be plotted to obtain a two-dimensional diagram of all possible visible chromaticities called the *xy-chromaticity diagram*. The two-dimensional chromaticity diagram demonstrates a linear relation between the colors when mixed additively as shown in Figure 3.4. A straight line drawn joining the chromaticity coordinates of any two colors that are mixed includes the

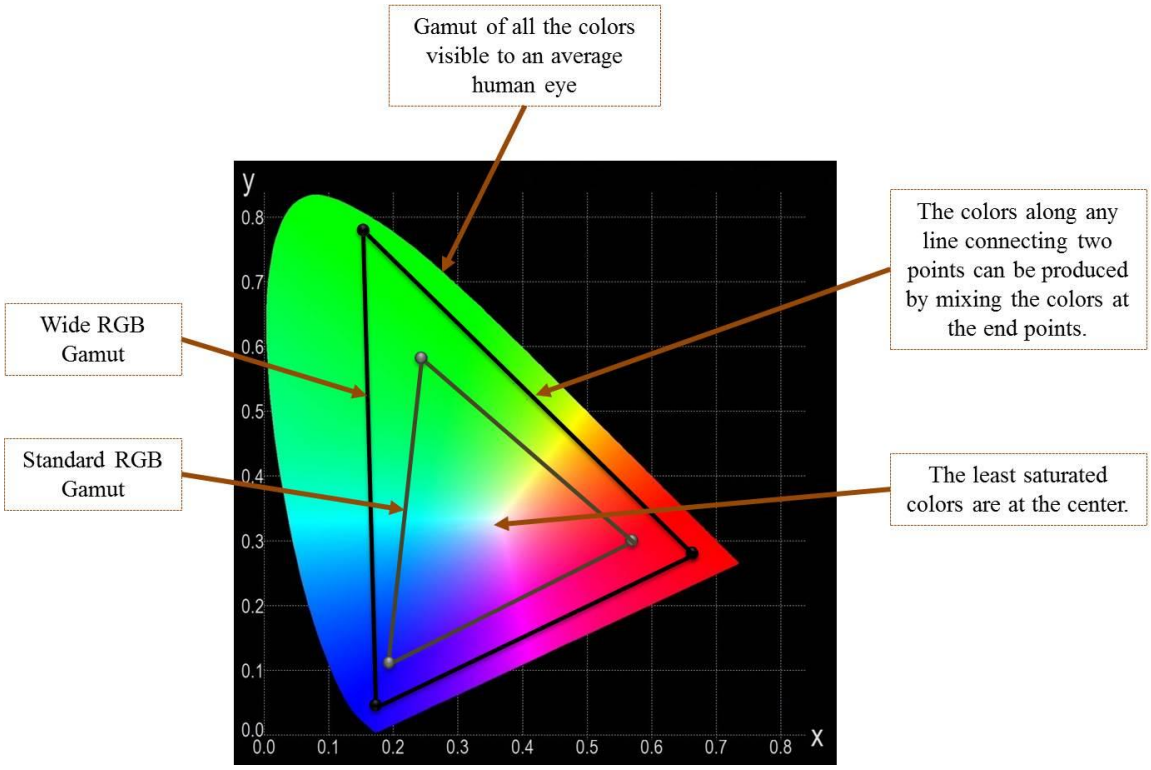

Figure 3.4 The CIE color space chromaticity diagram.

chromaticity coordinates of all possible colors of the mixture. In case three colors are mixed additively, all the colors that can be produced by mixing any fraction of those three colors lie within the triangular region on the diagram formed by connecting the (*x, y)* coordinates of the individual colors. The triangular region, thus formed, is called the *color gamut.*[6] The color gamut of a device or process is specified in the *hue-saturation plane* and is defined as that portion of the color space which can be reproduced. An unrealized goal within the color display engineering is a device that is able to reproduce the entire visible color space!

3.5 Results and Discussion

Colorful beetles have been studied by various research groups[8, 71-77] and it has been experimentally shown that the selective reflection of light by multifaceted

arrangement of photonic structures inside exoskeleton cuticle scales leads to the brilliant structural coloration.[14, 78] The weevil *E. chevrolati* belongs to one of the largest animal family with over 400 species all over the world, called *Curculionidae*. An average adult weevil is about 1 - 40 mm long and can be recognized by its elongated head that forms a snout and antennae with small clubs. These weevils have a somber yellowish-green appearance, as can be seen in Figure 2.3 (a).

In our research, we chose to study the *E. chevrolati* weevil because of the brilliant multicolored micron-sized domains in its scales with three-dimensional photonic crystal based internal structure. *E. chevrolati* proved to be an excellent model for:

a. studying the mechanism behind selective angle-independent reflectance from the structural architecture.
b. understanding its usual dull, pastel-type appearance, in spite of the presence of bright differently-colored domains on its exoskeleton.
c. producing the *color gamut*, range of reproducible colors, as observed by a standard human observer.

The range of colors which can be reproduced by the biological photonic structures was defined by following the same procedure for the calculation of the chromaticity coordinates *x* and *y*, as explained in Section 3.4. The color gamut for the *E. chevrolati* weevil (Figure 3.5) was defined on the CIE 1931 chromaticity diagram by considering differently-colored domains within its scales, and calculating the *xy*-chromaticity coordinates of the three individual domains as listed in Table 3.1. Figure 3.5 shows the corresponding *xy*-chromaticity diagram containing the coordinate points of selected domains of weevil scales.

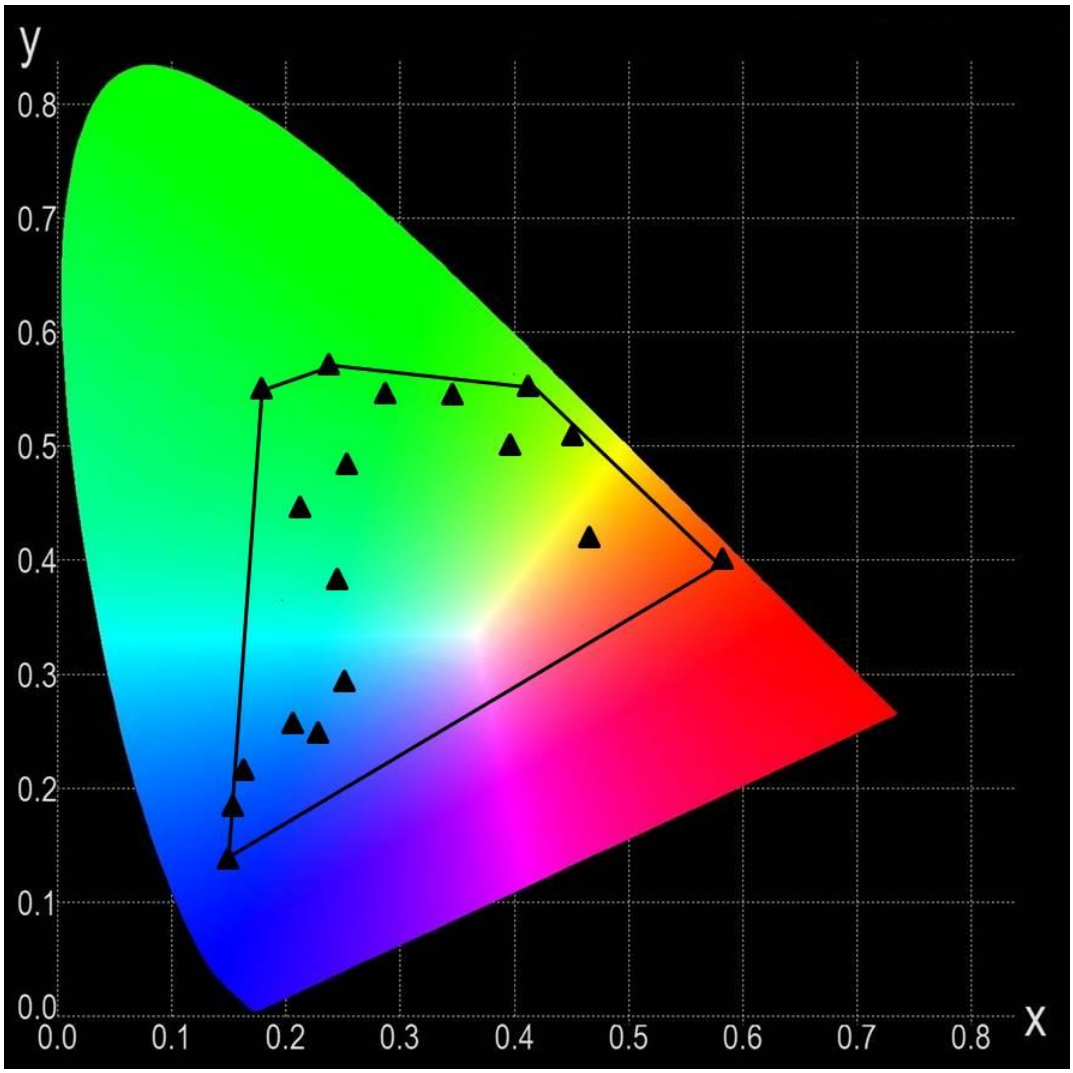

Figure 3.5 *xy*-chromaticity diagram for multicolored domains.

Table 3.1 *xy*-chromaticity coordinates for the individual domains on the weevil.

Scale No.	***x***	***y***
1	0.59	0.40
2	0.34	0.54
3	0.14	0.19
4	0.44	0.51
5	0.23	0.25
6	0.19	0.21
7	0.16	0.55
8	0.41	0.54
9	0.40	0.50
10	0.15	0.13
11	0.24	0.57
12	0.21	0.44
13	0.27	0.30
14	0.48	0.42
15	0.21	0.25
16	0.24	48
17	0.30	0.54
18	0.25	0.38

The area lying within the lines connecting the domain's chromaticity coordinates forms the *color gamut* for the weevil. This area represents all possible colors visible to an average human observer, which can be produced upon the incidence of light on these domains on the weevil. In contrast to the three-color RGB gamut in electronic display systems (TV screens[79], for example), these biological systems demonstrate a wide gamut of colors which can be reproduced by the additive-mixing of reflected lights from a number of colored domains spanning almost the entire visible wavelength range.

The calculated chromaticity coordinates corresponding to individual scales on the weevil are listed in Table 3.2. The corresponding locations in the *xy*-chromaticity diagram are shown in Figure 3.6. On comparing the chromaticity diagram for individual scales (Figure 3.6) with the one obtained for individual domains (Figure 3.5), we found that all the 'color' coordinates of individual scales lie within the color gamut produced for the three domains of red, green and blue-color. Interestingly, due to the low frequency of occurrence of blue domains within individual scales, the overall mixed color of individual scales is located far from the blue range in the *xy*-chromaticity diagram.

Similarly, when analyzing the color of a whole weevil (without resolving individual domains or scales), the color gamut is reduced to a single point in the yellowish-green area on the *xy*-chromaticity diagram, as shown in Figure 3.7. The chromaticity coordinates were calculated to be (0.43, 0.55) in excellent agreement to the observed uniform yellowish-green color of this weevil.

Detailed analysis of the color gamut produced in different size-levels suggested the additive mixing of primary colors occurring in the *E. chevrolati* weevils before the reflected colors are perceived by an observer.

Table 3.2 *xy*-chromaticity coordinates for the individual scales on the weevil *E. chevrolati*.

Scale No.	*x*	*y*
1	0.42	0.52
2	0.38	0.55
3	0.61	0.39
4	0.44	0.49
5	0.36	0.54

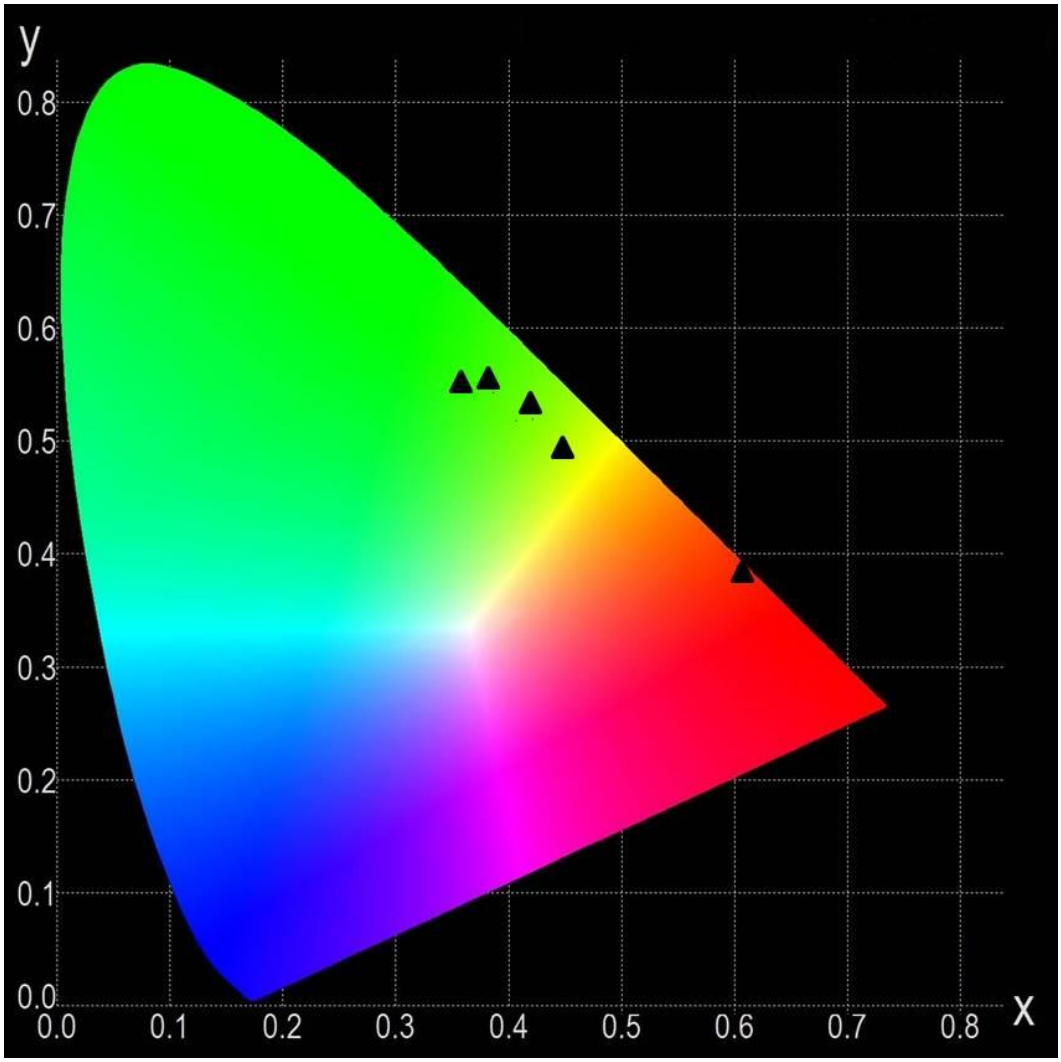

Figure 3.6 *xy*-chromaticity diagram for the weevil scales.

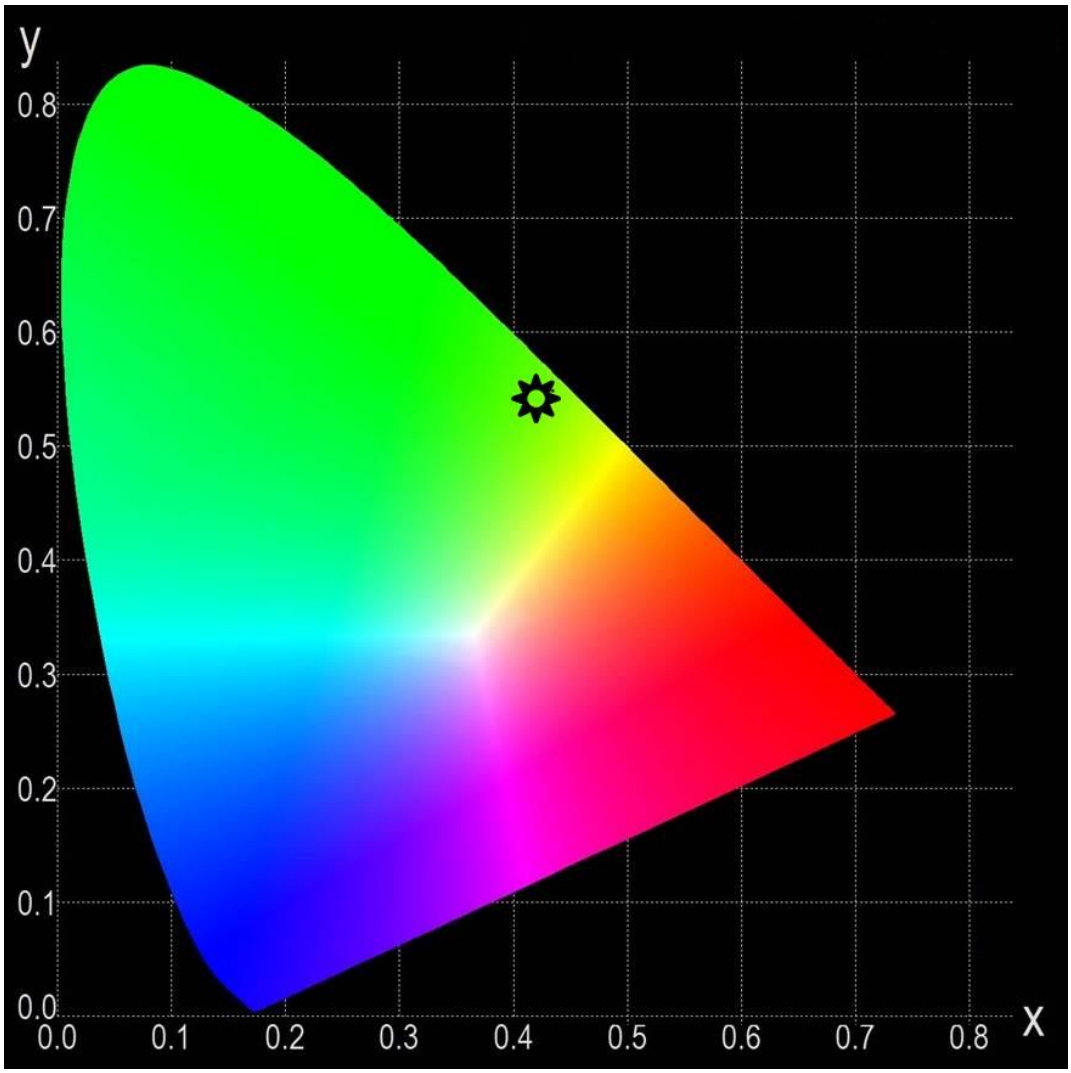

Figure 3.7 *xy*-chromaticity diagram for the whole weevil.

In addition to the color coordinate analysis, the color mixing in *E. chevrolati* weevils is further supported by their dull appearance. The weevil appears to be of dull yellowish-green color when viewed with an unaided eye from a distance but differently colored brilliant domains become visible when viewed under the microscope. This is a result of the *pointillistic color mixing* since the primary-colored domains are placed so close to one another on the weevil's exoskeleton that the reflected colors from these domains merge to generate a perception of other colors.[80] Patterns beyond the neural resolution limit[81] are removed from the retinal image by the optical system of the human eye.[82] *Pointillism* is a painting technique in which the individual bright dots of different hues are placed so that the color spots blend into a fuller range of tones.[83, 84] Most likely, this macroscopic dull yellowish-green appearance helps the weevil to hide in its surrounding habitat from its predators such as birds.[§85, 86]

The mathematical representation of colors (color modeling) and the physical phenomena taking place inside the human eye suggest that the colors reflected from the exoskeleton of the studied weevil are mixed additively before the color information is processed by the human brain. In spite of a wide range of colors produced by the photonic crystal structure inside the exoskeleton of weevil *E. chevrolati*, the human eye perceives only the final color resulting from the additive-mixture of lights of different colors.

3.6 Conclusions

We studied the weevil *E. chevrolati* using color theory and *xy*-chromaticity diagrams based on the CIE *XYZ* color model. We found the exoskeleton of the studied

[§] A typical bird eye responds to the wavelength range of about 300 - 700 nm in addition to the ultraviolet wavelength (300 – 400 nm).

weevil is studded with micron-sized brilliantly colored domains, arranged beautifully in a pixel-like alignment similar to that found in modern-day display systems. By carefully examining the weevil microscopically and by representing the observed colors mathematically with the help of color models and reflectance spectra measurements, we found that the perceived yellowish-green color of the weevil is a result of the additive color mixing of the reflected lights from the photonic structured domains in its scales. As a possible practical application, this micropixelation and color mixing in the biological photonic structures, where the individual domains serve as primary color sources, can be replicated synthetically to be used in the RGB LED lighting designing, which consists of a red, a green and a blue LED, and delivers a color gamut to screens. Also, the distance between the red, green and blue points can be increased to reproduce more vivid colors, much similar to the *pointillistic color mixing technique.*

CHAPTER 4

SUMMARY AND CONCLUDING REMARKS

We have studied the chromatic effects in biological three-dimensional photonic crystal structures (iridescent exoskeleton scales of a weevil) operating at visible wavelengths by a range of experimental and modeling techniques. The optical and structural properties of the biological photonic crystal were studied by high-resolution scanning microreflectance spectroscopy, focused ion beam milling and scanning electron microscopy. From these structural insights the photonic band structure was determined using MIT's MPB software that combines Maxwell's equations with solid-state physics concepts. In addition, the peculiar pointillistic coloration scheme of the weevil was investigated using colorimetric[**] concepts, and an interesting color-mixing strategy was discovered.

We found that the structural coloration in the weevil *E. chevrolati* is a consequence of the structural arrangement of individual color-producing elements, referred to as photonic *domains*, which contain the same photonic crystal lattice structure but slightly different lattice parameters (varying between 360 and 400 nm) and crystal orientations. The weevil's exoskeleton is a multicomponent representation of micron-sized photonic structures with varying dimensions.

[**] Science used to quantify and describe physically the color perception of a human observer.

The photonic architecture was investigated by optical and structural techniques. Our reflectance measurements for the weevil's hierarchical structure consisted of multiple levels: domains, scales and exoskeleton. These detailed, hierarchical studies confirmed the proposed *theory of additive color mixing* as the reason behind the yellowish-green coloration of the weevil. We observed that the reflectance spectrum of a large section of the weevil encloses the peak reflectance maxima positions for the individual domains and the scales.

On the microscopic level, we investigated the three-dimensional structure of the photonic crystal within each domain using the high-resolution cutting and imaging techniques such as focused ion beam milling and scanning electron microscopy. These studies provided us with the lattice dimensions and existing internal structural organization and presented the basis for three-dimensional structural modeling and photonic band structure calculations. Using MIT's photonics bands software, the forbidden frequencies ranges for light propagation in the weevil's photonic crystal structure were determined. In detail, we first compared the internal photonic structure (from electron microscopy imaging) with the cross-sectional images of the cuts through the re-constructed three-dimensional dielectric model (obtained from band structure calculations) based on face-centered cubic lattice structure along specific directions. We found good overlap between the two-dimensional model crystal faces with the structural images, confirming the ABC stacked layers of air cylinders ordered in a *fcc-cubic lattice* in a dielectric material.

The calculated photonic band structure of the weevil's photonic crystal possesses stop-gaps in all main lattice directions (L-Γ, Γ-X, Γ-U, Γ-W and Γ-K). It was discovered

that irrespective of the lattice constant value, longer wavelengths (reds) were generated only from the Γ-L direction, whereas the shorter ones (violets) were forbidden to enter the crystal in the Γ-W and Γ-K directions. We observed that the *maximum range of colors* that can be produced by a particular domain depends on the value of lattice constant. We found that photonic structures inside the exoskeleton of the weevil based on different lattice constants of 360 nm, 380 nm and 400 nm yield overall wavelength ranges between 441 – 585 nm, 465 – 618 nm and 490 – 650 nm, respectively (as listed in Table 2.1). This result suggests that the sophisticated microdomain orientation of the fcc-based photonic structures of the weevil *E. chevrolati* generates a minimum wavelength of ~441 nm (violet region of electromagnetic spectrum) and a maximum of ~650 nm (the red region). This is in excellent agreement with our optical reflectance spectroscopy results for individual domains, with a minimum observed wavelength of ~442 nm and a maximum of ~657 nm (see Figure 2.7).

As a major contribution of this thesis, we tested our hypothesis of *additive color mixing* in biological photonic structures by representing the observed colors on the mathematically-defined color space, *CIE XYZ color space*. We produced the color gamut for different structural levels (domains, scales, exoskeleton) by calculating the chromaticity coordinates (x, y) for a set of 18 individual domains and 5 different scales. This numerical analysis of generated colors at the microscopic level and its comparison to the macroscopic level, the weevil's exoskeleton, suggests the mixing of colors before they are observed by a human observer. With regards to the observed dull yellowish-green appearance of the weevil, our hypothesis is that it is a result of the blend of all the pointillistic colors reflected from the weevil's multicolored domains, which are placed in

close proximity to each other, before the individual color details are identified and processed by the human brain.

REFERENCES

1. A. R. Parker, J. Opt. A. Pure Appl. Opt. 2 (6), R15-R28 (2000).

2. S. Kinoshita, S. Yoshioka and J. Miyazaki. Rep. Prog. Phys. 71 (7), 076401 (2008).

3. M. G. Meadows, M. W. Butler, N. I. Morehouse, L. A. Taylor, M. B. Toomey, K. J. McGraw and R. L. Rutowski. J. R. Soc. Interface 6 (Suppl 2), S107-S113 (2009).

4. L. D'Alba, V. Saranathan, J. A. Clarke, J. A. Vinther, R. O. Prum and M. D. Shawkey. Biol. Lett. 7 (4), 543-546 (2011).

5. P. Vukusic and J. R. Sambles. Nature 424 (6950), 852-855 (2003).

6. M. Srinivasarao. Chem. Rev. 99 (7), 1935-1962 (1999).

7. J. W. Galusha, L. R. Richey, M. R. Jorgensen, J. S. Gardner and M. H. Bartl. J. Mater. Chem. 20 (7), 1277-1284 (2010).

8. A. E. Seago, P. Brady, J.-P. Vigneron and T. D. Schultz. J. R. Soc. Interface 6 (Suppl 2), S165-S184 (2009).

9. S. M. Doucet and M. G. Meadows. J. R. Soc. Interface 6 (Suppl 2), S115-S132 (2009).

10. P. Vukusic, J. Sambles, C. Lawrence and R. Wootton. Proc. R. Soc. London, Ser. B: Biological Sciences 266 (1427), 1403-1411 (1999).

11. D. Osorio and A. Ham. J. Exp. Biol. 205 (14), 2017-2027 (2002).

12. S. Kinoshita and S. Yoshioka. ChemPhysChem 6 (8), 1442-1459 (2005).

13. V. Welch, V. Lousse, O. Deparis, A. Parker and J. P. Vigneron. Phys. Rev. E 75 (4), 041919 (2007).

14. J. W. Galusha, L. R. Richey, J. S. Gardner, J. N. Cha and M. H. Bartl. Phys. Rev. E 77 (5), 050904 (2008).

15. K. Gromysz-Kałkowska and A. Unkiewicz-Winiarczyk. Annales UMCS, Biologia (2010).

16. J. P. Caldwell. J. Zool. 240 (1), 75-101 (1996).

17. W. Schuler and E. Hesse. Behav. Ecol. and Sociobiol. 16 (3), 249-255 (1985).

18. E. B. Poulton. The colours of animals: their meaning and use, especially considered in the case of insects. (D. Appleton and Company, 1890), pp. 159-215.

19. http://ab-initio.mit.edu/photons/tutorial/

20. E. Yablonovitch. Phys. Rev. Lett. 58 (20), 2059-2062 (1987).

21. E. Yablonovitch, T. J. Gmitter and K. M. Leung. Phys. Rev. Lett. 67 (17), 2295-2298 (1991).

22. S. G. Johnson and J. Joannopoulos. Appl. Phys. Lett. 77 (22), 3490-3492 (2000).

23. J. D. Joannopoulos, R. V. Pierre and F. Shanhui. Nature 386 (6621), 143-149 (1997).

24. M. G. Han, C.-J. Heo, H. Shim, C. G. Shin, S.-J. Lim, J. W. Kim, Y. W. Jin and S. Lee. Advanced Optical Materials 2 (6), 535-541 (2014).

25. L. Rayleigh. Philos. Mag. Series 5 24 (147), 145-159 (1887).

26. S. John. Physical Rev. Lett. 58 (23), 2486-2489 (1987).

27. T. F. Krauss, R. De La Rue and S. Brand. Nature 383 (6602), 699-702 (1996).

28. J. C. Knight, T. A. Birks, P. S. J. Russell and J. G. Rarity. Appl. Opt. 37 (3), 449-452 (1998).

29. G. Floquet. Ann. ENS [2] 12, 47-88 (1883).

30. S. G. Johnson and J. D. Joannopoulos. Photonic Crystal Tutorial, 1-16 (2003).

31. J. D. Joannopoulos, S. G. Johnson, J. N. Winn and R. D. Meade. Photonic crystals: molding the flow of light. (Princeton University Press, 2011).

32. M. Maldovan and E. L. Thomas, Periodic Materials and Interference Lithography (Wiley-VCH Verlag GmbH & Co., 2009), pp. 168-172.

33. S. Johnson and J. Joannopoulos. Opt. Express 8 (3), 173-190 (2001).

34. J. Mollon, J. Bowmaker and G. Jacobs. Proc. R. Soc. London, Ser. B: Biological Sciences 222 (1228), 373-399 (1984).

35. A. Hudson, E. M. Press and N. Lewiston. Perception 41, 626-630 (2012).

36. D. M. Hunt, K. S. Dulai, J. A. Cowing, C. Julliot, J. D. Mollon, J. K. Bowmaker, W.-H. Li and D. Hewett-Emmett. Vision Res. 38 (21), 3299-3306 (1998).

37. G. Halder, P. Callaerts and W. J. Gehring. Curr. Opin. Genet. Dev. 5 (5), 602-609 (1995).

38. A. K. Surridge, D. Osorio and N. I. Mundy. Trends in Ecology & Evolution 18 (4), 198-205 (2003).

39. M. R. Pointer and G. G. Attridge. Color Res. Appl. 23 (1), 52-54 (1998).

40. J. Mollon, O. Estevez and C. Cavonius. Vision: coding and efficiency, 119-131 (1990).

41. J. K. Bowmaker. Eye (London, England) 12 (Pt 3b), 541-547 (1998).

42. G. H. Jacobs. Philos. Trans. R. Soc. B: Biological Sciences 364 (1531), 2957-2967 (2009).

43. I. Newton and N. Chittenden. Newton's principia: the mathematical principles of natural philosophy. (D. Adee, 1848).

44. I. Newton. Philos. Trans. (1665-1678), 3075-3087 (1965).

45. J. C. Maxwell. Philos. Trans. R. Soc. London 150, 57-84 (1860).

46. T. Young. Philos. Trans. R. Soc. London 91, 23-88 (1801).

47. G. H. Jacobs. Biol. Rev. 68 (3), 413-471 (1993).

48. C. CIE, Commission Internationale de l'Eclairage Proceedings, 1931 (Cambridge University Press Cambridge, 1932).

49. T. Smith and J. Guild. Trans. Opt. Soc. 33 (3), 73-134 (1931).

50. C. Lueck, S. Zeki, K. Friston, M.-P. Deiber, P. Cope, V. J. Cunningham, A. Lammertsma, C. Kennard and R. Frackowiak. Nature 340, 386-389 (1989).

51. A. Bartels and S. Zeki. Eur. J. Neurosci. 12 (1), 172-193 (2000).

52. H. R. Swanzy. The BMJ 2 (1455), 1089-1096 (1888).

53. J. Schanda. Colorimetry: understanding the CIE system. (John Wiley & Sons, 2007), pp. 25-34.

54. N. Ohta and A. Robertson. Colorimetry: fundamentals and applications. (John Wiley & Sons, 2006); pp. 1-114.

55. M. Luckiesh. Color and its applications. (D. Van Nostrand Company, 1921, pp. 1-86.

56. K. Nassau. Color for science, art and technology. (Elsevier, 1997), pp. 11-17.

57. S. Jennings. Artist's Color Manual: the complete guide to working with color. (Chronicle Books, 2003), p. 21.

58. S. K. Shevell. The science of color. (Elsevier, 2003), pp. 26-29.

59. D. R. Proffitt. Curr. Dir. Psychol. 15 (3), 131-135 (2006).

60. J. C. Russ. The image processing handbook. (CRC press, 2010), p. 94.

61. P. Riordan-Eva. Vaughan & Asbury's General Ophthalmology, 18e, edited by P. Riordan-Eva and E. T. Cunningham (The McGraw-Hill Companies, New York, NY, 2011), Chapter 1.

62. M. A. Ali, M. A. Klyne and K. Tansley. Vision in vertebrates. (Springer, 1985), p. 28.

63. R. G. Boothe. Perception of the visual environment. (Springer, 2002), p. 200.

64. T. Young. Philos. Trans. R. Soc. London 92, 12-48 (1802).

65. C. L. Lerea, A. H. Bunt-Milam and J. B. Hurley. Neuron 3 (3), 367-376 (1989).

66. J. Hirsch and C. A. Curcio. Vision Res. 29 (9), 1095-1101 (1989).

67. M. D. Fairchild. Color appearance models. (John Wiley & Sons, 2013), pp. 76-77.

68. C. Poynton. Digital video and HD: algorithms and interfaces. (Elsevier, 2012), p. 219.

69. F. W. Billmeyer and M. Saltzman. Principles of color technology, 2nd ed. (J. Wiley & sons, 1981), Chapter 2.

70. G. Wyszecki and W. S. Stiles. Color science: concepts and methods,quantitative data and formulae, 2nd ed. (Wiley New York, 1982).

71. M. E. McNamara, D. E. G. Briggs, P. J. Orr, H. Noh and H. Cao. Proc. R. Soc. Ser. B: Biological Sciences, 1114-1121 (2011).

72. L.P. Jiang, B. Q. Dong, X. H. Liu, F. Liu and J. Zi, Chin. Sci. Bull. 57 (24), 3211-3217 (2012).

73. S. Yoshioka, S. Kinoshita, H. Iida and T. Hariyama. J. Phys. Soc. Jpn. 81 (5), 054801-1 - 054801-7 (2012).

74. V. Sharma, M. Crne, J. O. Park and M. Srinivasrao. Science 325 (5939), 449-451 (2009).

75. JF. Colomer, P. Simonis, A. Bay, P. Cloetens, H. Suhonen, M. Rassart, C. Vandenbem and J. P. Vigneron. Phys. Rev. E 85 (1), 011907-1 - 011907-9 (2012).

76. B. Q. Dong, T. R. Zhan, X. H. Liu, L. P. Jiang, F. Liu, X. H. Hu and J. Zi1. Phys. Rev. E 84 (1), 011915-1 -011915-5 (2011).

77. F. Liu, B. Q. Dong, X. H. Liu, Y. M. Zheng and J. Zi. Opt. Express 17 (18), 16183-16191 (2009).

78. J. W. Galusha, L. R. Richey and M. H. Bartl. Presented at the IEEE/LEOS Summer Topical Meetings, 2008 Digest of the, 2008 (unpublished).

79. A. R. Smith. Presented at the ACM Siggraph Computer Graphics, 1978 (unpublished).

80. N. Krüger, F. Wörgötter. Leonardo 38 (4), 337-340 (2005).

81. J. Beynon. Phys. Educ. 20 (5), 234-237 (1985).

82. F. Campbell, R. Gubisch. J. Physiol. 186 (3), 558-578 (1966).

83. R. S. Berns, S. Byrns, F. Casadio, I. Fiedler, C. Gallagher, F. H. Imai, A. Newman and L. A. Taplin. Color Res. Appl. 31 (4), 278-293 (2006).

84. G. F. Jenks. Prof. Geogr., 5, 4-6 (1953).

85. T. H. Goldsmith. Sci. Am. 295 (1), 68-75 (2006).

86. S. Wilkie, P. Vissers, D. Das, W. Degrip, J. Bowmaker and D. Hunt. Biochem. J., 330, 541-547 (1998).